Winterer, E.L., Sager, W.W., Firth, J.V., and Sinton, J.M. (Eds.), 1995
Proceedings of the Ocean Drilling Program, Scientific Results, Vol. 143

15. PETROLOGY AND GEOCHEMISTRY OF IGNEOUS ROCKS FROM ALLISON AND RESOLUTION GUYOTS, SITES 865 AND 866[1]

P.E. Baker,[2] P.R. Castillo,[3] and E. Condliffe[2]

ABSTRACT

At Site 866 (Resolution Guyot), the volcanic basement (>1620 mbsf and <128 Ma) consists of a series of subaerial lava flows separated by scoriaceous, rubbly, and clay (iron-rich smectite) intervals. The lavas may be divided into three main groups on petrographic and geochemical grounds. Because of alteration, the geochemical evidence depends mainly on relatively immobile elements, such as Ti, Zr, Nb, and the rare earth elements. The lowest group (>1727 mbsf) is picritic and alkalic (high Nb/Ti and Nb/Zr). The middle group (1673–1727 mbsf), with megacrysts and phenocrysts of plagioclase, olivine, and clinopyroxene, is more markedly alkalic (e.g., steep mid-ocean ridge basalt-normalized light rare earth element-enriched patterns). The upper group (above 1673 mbsf) includes basalts rich in plagioclase megacrysts overlain by picrites, and is more tholeiitic (lower Nb/Ti, Zr/Ti, and flatter rare earth element patterns). At Site 865 (Allison Guyot), altered basaltic sills are intrusive into Albian clayey dolomitic limestones between 830 and 870 mbsf. Several lines of evidence indicate that the sediment was unconsolidated at the time of invasion by the basalt (<111 Ma). Salitic clinopyroxenes, abundances and ratios of the less mobile incompatible elements, and pronounced light rare earth element-enrichment all point to a decidedly more alkalic affinity than was seen at Site 866. Resolution and Allison guyots probably originated within the region of intense hotspot volcanism referred to as the South Pacific isotopic and thermal anomaly or SOPITA. The two guyots probably followed a similar tectonic pathway and may have passed over more than one hotspot. Geochemical evidence (e.g., Nb/Zr and Zr/Ti) suggests that they have more in common with the Society-Austral (Tubuai) Islands than with islands to the east (e.g., Marquesas, Easter) or the west (Cook, Samoa): this is also consistent with lineaments derived by backtracking.

INTRODUCTION

A vast area of the South Pacific Ocean, about 3000 km across, was the site of intense mid-plate volcanism during the Early Cretaceous. The location of this activity probably corresponds with the present-day South Pacific Superswell (McNutt and Fischer, 1987), which includes the Society, Cook, and Austral archipelagos. It also belongs to SOPITA, the area of the so-called South Pacific isotopic and thermal anomaly (Staudigel et al., 1991). The lavas of these islands also form part of the isotopically distinct Southern Hemisphere belt referred to as the Dupal Anomaly (Hart, 1984). In the western part of the Mid-Pacific Mountains (MPM), a series of broad plateaus is surmounted by flat-topped seamounts. The age of the oceanic crust beneath the MPM is estimated to be about 119 to 130 Ma near Allison Guyot and may be as old as 154 Ma farther west, around Resolution Guyot (Sager, Winterer, Firth, et al., 1993). The guyots are capped by shallow-water limestones of Barremian–Albian age (124–98 Ma). The Cretaceous seamounts of the MPM probably formed over the South Pacific Superswell and were translated northwestward on zig-zag pathways, determined by changes in plate motion, to their present location (Fig. 1). From the hotspot lineaments calculated by Duncan and Clague (1985), the seamounts of Sites 865 and 866 lie close to the Easter Island track, but would have passed near the Marquesas and Society hotspots during their transit. A period of rejuvenation and uplift may have accompanied their passage over these other hotspots. The ages calculated by Duncan and Clague (1985) are consistent with the location of the guyots over the Marquesas or Society hotspots at 100 to 120 Ma.

Site 866 is discussed first, as it represents a substantial section through volcanic basement and was the only instance where basement was reached during Leg 143. At Site 865, on Allison Guyot, igneous rocks are confined to a group of basaltic sills intruded into the sediments. Some comparisons are made with a few samples from Site 869, on a sediment apron extending southward from Wodejebato Guyot and Pikinni Atoll. The detailed petrology and geochemistry of the volcaniclastics from Site 869 are treated separately (see Janney et al., this volume).

ANALYTICAL METHODS

X-ray fluorescence (XRF) analyses for major and trace elements (excluding rare earth elements) were conducted at the Department of Earth Sciences, Leeds University, using a wavelength-dispersive automated Philips PW 1400 spectrometer. Major elements were determined on fused glass beads and trace elements on pressed powder pellets. Accuracy and precision for major elements are estimated at better than 3% for Si, Ti, Fe, Ca, and K and 7% for Mg, Na, Al, Mn, and P: for trace elements above 10 ppm they are estimated at better than 10%. Rare earth element (REE) determinations were performed on a VG Instruments PlasmaQuad II+ inductively coupled plasma mass spectrometer (ICPMS) at the Scripps Institution of Oceanography. Multiplier voltage was set at 5 kV and nebulizing gas flow rate at 0.2 L/m. ^{115}In was used as an internal standard, and calibration was conducted using standard solutions of 5, 10, 50 and 100 ppb REE. Accuracy and precision of the analyses were monitored using the rock standards AGV-1 and BCR-1. Rock powders (0.014 g) were dissolved in clean Teflon vessels using ≈1 mL 2:1 mixture of concentrated HF and HNO_3 and then heated overnight over a hot plate at low temperature. The resulting solution was evaporated to dryness, resuspended in a small amount of concentrated HNO_3, and evaporated to dryness, and finally diluted to a factor of 1000 in a 1% HNO_3 solution containing 100 ppb ^{115}In. Accuracy of the analyses, based on repeated measurements of BCR-1 and AGV-1 standards, is better than 5%, especially for the light elements.

Microprobe analyses were performed using a CAMECA SX-50 instrument fitted with three wavelength dispersive spectrometers and a LINK 10/55S energy dispersive system. Analysis conditions were as follows:

[1] Winterer, E.L., Sager, W.W., Firth, J.V., and Sinton, J.M. (Eds.), 1995. *Proc. ODP, Sci. Results,* 143: College Station, TX (Ocean Drilling Program).
[2] Department of Earth Sciences, University of Leeds, Leeds LS2 9JT, United Kingdom.
[3] Geological Research Division, Scripps Institution of Oceanography, University of California, San Diego, La Jolla, CA 92093-0220, U.S.A.

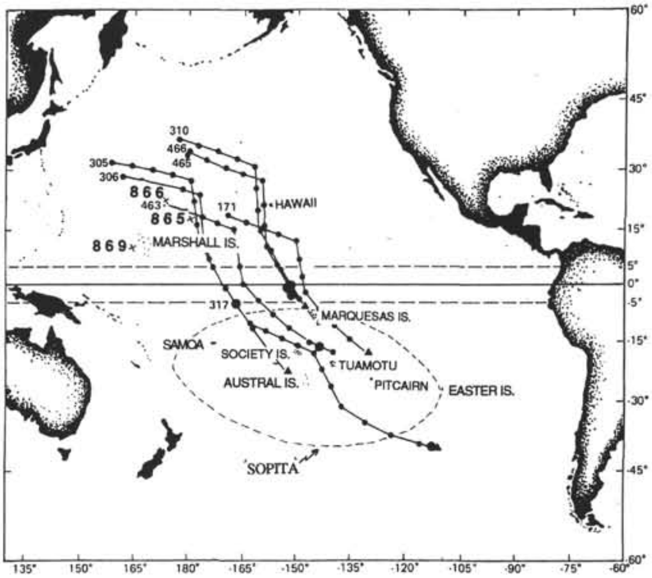

Figure 1. Location of Allison (Site 865) and Resolution (Site 866) guyots in relation to island groups and hotspot lineaments of the South Pacific (after Shipboard Scientific Party, 1981). Approximate location of SOPITA after Palacz and Saunders (1986).

1. Silicates and opaque oxides, excluding feldspars: beam energy, 15 kV; beam current, 15 nA; count times, Na, Mg, Al, Si, K, Ca, Ti, all 15 s on peak and 10 s on background; Cr, Mn, Fe, Ni, 30 s on peak and 20 s on background.
2. Feldspars: beam energy, 15 kV; beam current, 10 nA. Count times for all elements: 10 s on peak and 10 s on background. Where necessary, beam broadened to 2 or 3 µm to prevent excessive element loss.
3. Raw counts were corrected for inter-elemental effects using CAMECA proprietary software.
4. Standards used: Na, albite; Mg, spinel; Al, kyanite; Si, diopside; K, orthoclase; Ca, wollastonite; Ti, sphene; Cr, chromite; Mn, rhodonite; Fe, haematite; and Ni, nickel oxide.

SITE 866

Resolution Guyot (21°19.9′N, 174°18.8′E) lies in 1373 m of water and consists of a 1620-m cap of shallow-water carbonates and pelagic sediments that rests on a topographically subdued volcanic structure rising only about 0.5 km above the general level of the MPM plateau. K/Ar whole-rocks, whose ages inevitably are suspect with such highly altered states, yield ages in the range of 107 to 125 Ma (Pringle et al., this volume). On the other hand, $^{40}Ar/^{39}Ar$ dates by the same authors give ages in the range of 120 to 129 Ma (i.e., mid-Barremian to mid-Aptian on Harland et al.'s [1990] time scale). Errors in the measurements are such that it is not possible to be certain whether this represents a simple succession of lava flows or whether there are also some intercalated sills. However, the new petrographic and geochemical data presented here show substantial petrologic variations in the basement of Resolution Guyot. It is now thought likely that the 125-m-thick volcanic sequence drilled at Site 866, originally interpreted as exclusively lava flows separated by rubbly intervals (Fig. 2), may contain some intrusive bodies. The average thickness of the flows and sills is estimated at about 10 m, but poor recovery of the contacts and the friable nature of the interbasaltic beds probably means that they have been underestimated. The interbasaltic intervals range from clays to clast- or matrix-supported breccias in which the clasts are subangular to subrounded fragments of vesicular and amygdaloidal basalt, similar to the associated lava flows and sills. The matrix generally consists of reddish sandy clay; distinct layers of red clay also are found within the breccias (e.g., at interval 143-866A-180R-5, 54–57 cm). Fractures and cavities within the breccias also may be filled with red clay. X-ray diffraction (XRD) analysis of the clay indicates that it is an iron-rich smectite; some kaolinite also has been identified.

Most of the interbasaltic intervals are considered to be the products of various processes operating on a tropical or subtropical volcanic land surface. Each such interval probably represents decades or centuries as opposed to the span of perhaps hours or days required for emplacement of a single lava flow. Some of the interbasaltic intervals may represent oxidized soils, boles, or lateritic horizons. Other intervals probably represent the oxidized rubbly surface of aa flows, where weathering products have washed down to fill the intervening spaces. Some breccias may have formed as screes or been redistributed as mudflows or debris slides, but others may have been caused by the intrusion of sills. The fractured and porous nature of the Unit 7 breccia provided access for hydrothermal fluids and their precipitates. Veins and cavities are commonly filled with calcite, zeolites, clay minerals, and analcime.

Petrography

In the Leg 143 *Initial Reports* volume (Sager, Winterer, Firth, et al., 1993), the volcanic succession was divided into 12 units on the basis of the stratigraphic incidence of what originally were thought to be exclusively flows and interbasaltic intervals, without implying that these necessarily coincided with any petrographic differences. As a result of subsequent, and more detailed, investigations, petrographic and mineralogical compositional distinctions have now been drawn in respect of the lavas and sills and are shown in Figure 2. In summary, the different members are as follows:

Unit 1: A highly pyritized and calcified feldspathic basalt at the contact of the volcanic sequence with the overlying oolitic grainstone.

Unit 2: A very highly altered basalt containing abundant ilmenite and titanomagnetite in a matrix of alkali feldspar (e.g., Sample 143-866A-171R-3, 70–73 cm)

Unit 5: An olivine-phyric basalt with about 7% fresh olivine phenocrysts (Fo_{87-75}, <3 mm) and smaller plagioclase laths (An_{68-46}, <0.5 mm) in a matrix of clinopyroxene ($Ca_{46}Mg_{38}Fe_{16}$), magnetite, and feldspar. Cr-spinel crystals also occur (e.g., Sample 143-866A-177B-1, 1–3 cm).

Unit 6: This is distinguished by the abundance (15%) of plagioclase megacrysts and phenocrysts. Plagioclase megacrysts (<10 mm, An_{81-36}) are accompanied by smaller plagioclase laths (<2 mm, ~An_{68}) and olivines (<3 mm, Fo_{82-67}). Examples of these plagioclase-phyric basalts are Samples 143-866A-180R-3, 116–20 cm, and -180R-4, 1–4 cm).

Units 8–11: Plagioclase megacrysts and/or phenocrysts are again common (~5%) in this group, but less abundant than in the overlying basalt described in Unit 6. The large plagioclases (An_{71-63}) are locally accompanied by olivine (Fo_{86-74}) and clinopyroxene megacrysts ($Ca_{45}Mg_{41}Fe_{13}$). Examples are Samples 143-866A-182R-1, 102–105 cm, and -185R-3, 88–92 cm.

Unit 12: Olivine-phyric basalt, similar to that of Unit 5. Olivines (<3 mm) make up about 8% of the volume and are accompanied by scattered feldspar megacrysts (<6 mm). Olivine compositions are in the range Fo_{83-76}, and the feldspars are about An_{70}. As in Unit 5, some Cr-spinels occur. Interstitial groundmass feldspar has a composition of $Or_{19}Ab_{71}An_{10}$.

Mineral Chemistry

A wide range of *feldspar* compositions is represented in the Resolution Guyot volcanic succession. Megacrysts and phenocrysts of plagioclase are common throughout the sequence of lavas. Zoned, mostly within the labradorite range, they attain their most calcic com-

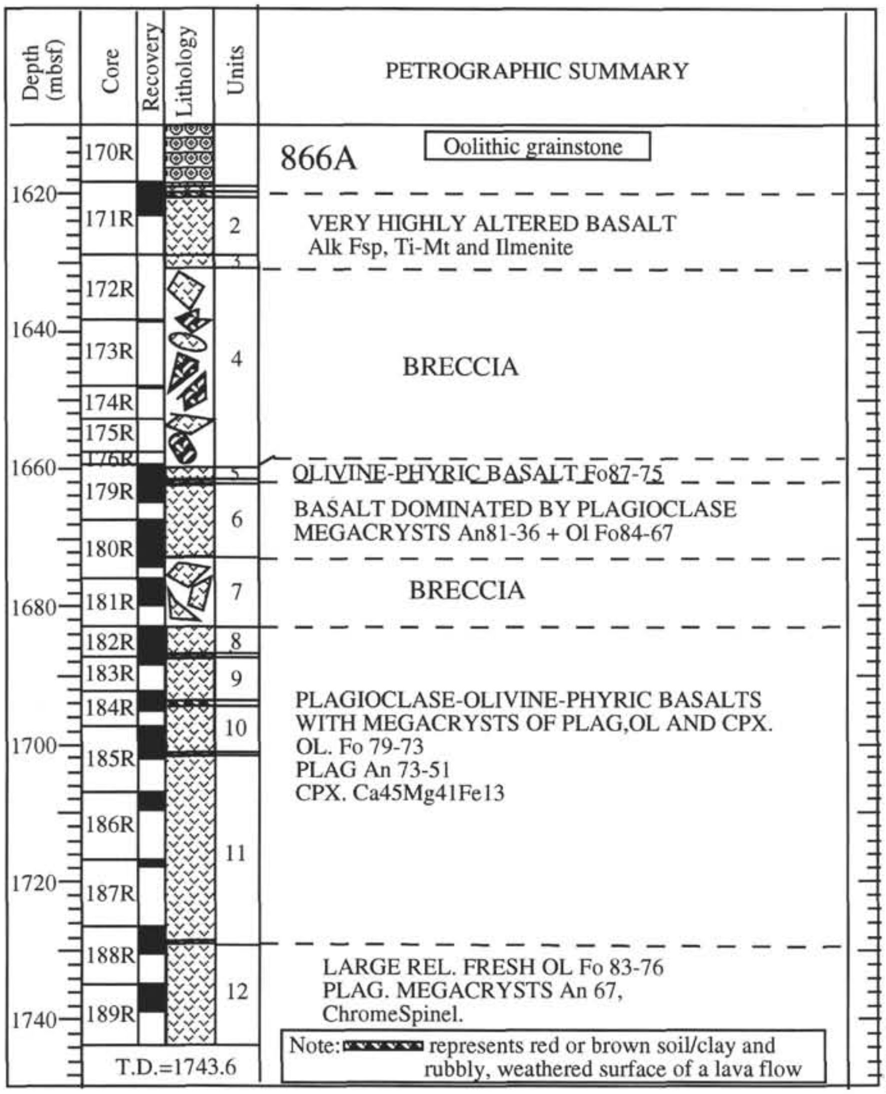

Figure 2. Stratigraphic succession in the volcanic basement of Resolution Guyot (Hole 866A) indicating major petrographic groupings distinguished within the lavas.

position (An_{81}) in the feldspar-phyric lavas of Unit 6. The wide range of feldspar compositions (Fig. 3 and Table 1) is partly attributable to magmatic processes, but probably also is the consequence of submarine weathering and exchange. Some interstitial groundmass feldspar is of albite composition and some is almost pure K-feldspar.

Olivine is invariably partially altered to, or wholly pseudomorphed by, serpentine minerals and iron oxides. The most magnesian compositions occur in lavas where olivine attains its maximum modal abundance (i.e., Unit 5 [Fo_{87}] and Unit 12 [Fo_{83}]). Phenocrysts are normally zoned to a minimum forsterite content of Fo_{65} at the rims (Table 2).

Clinopyroxene occurs as megacrysts in the central part of the volcanic sequence (Units 8–11), and occasionally appears as microphenocrysts; it is also a ubiquitous groundmass constituent. The clinopyroxene megacrysts in Sample 143-866A-182R-1, 102–105 cm, have a composition of $Ca_{45}Mg_{42}Fe_{13}$. In Sample 143-866A-185R-3, 88–92 cm, the megacrysts show sector zoning from $Ca_{43}Mg_{42}Fe_{15}$ to $Ca_{41}Mg_{34}Fe_{25}$, the latter being the most iron-rich pyroxene composition in the Resolution Guyot volcanics. A typical groundmass composition is $Ca_{44}Mg_{39}Fe_{17}$ (Sample 143-866A-177B-1, 1–3 cm). Projections of pyroxene compositions in terms of relative proportions of Ca-Mg-Fe (Fig. 4) show a concentration of points in the augite field with a small scattering toward Ca depletion and Fe enrichment. There is remarkably little overlap with the clinopyroxenes of Sites 865 and 869. Schweitzer et al. (1979) demonstrated how differences in pyroxene composition reflect differences in the type of basalt in which they occur. They point, for example, to higher Cr_2O_3 and lower TiO_2 in tholeiitic as opposed to alkalic pyroxenes. Higher TiO_2 and lower Cr_2O_3 concentrations occur in the pyroxenes from Hole 865A as compared with Hole 866A (Fig. 5 and Tables 3 and 4), indicative of the more alkalic nature of the former. The Site 866 pyroxenes tend to be concentrated in the augite field with a trend toward subcalcic ferroaugite. Fodor et al. (1975) demonstrated the different chemical characteristics of pyroxenes from the tholeiitic, alkalic, and nephelinic suites of Hawaii. On the ternary diagram (Fig. 4), pyroxenes of Site 865 plot largely in the salite field and are generally more calcic than those of Site 866. A high Wo component in clinopyroxenes has been shown by both Le Bas (1962) and Fodor et al. (1975) to be a feature of highly alkalic or nephelinic lavas.

Oxide phases are mainly titanomagnetite, but include ilmenite (e.g., Samples 143-866A-177B-1, 1–3 cm and -185R-2, 62–66 cm) and chrome spinel (e.g., Sample 143-866A-185-3, 88–92 cm) (Table 5).

Much of the *matrix* of the lavas has been altered to smectite, as confirmed by XRD. Electron microprobe analysis (e.g., 21% FeO and 15% MgO in Sample 143-866A-181-3, 91–96 cm) indicates an iron- and magnesium-rich clay, approximate in composition to ferroan saponite.

Table 1. Representative microprobe analyses (wt% oxide) and atomic proportions of feldspars in basaltic rocks from Holes 865A and 866A.

Core, section:	865A-94R-4	865A-93R-3	865A-93R-3	865A-91R-1	866A-189R-1	866A-186R-3	866A-185R-3	866A-182R-3	866A-182R-1	866A-180R-4	866A-180R-3
Interval (cm):	78–80	13–17	13–17	128–130	66–69	12–15	88–92	48–51	102–105	1–4	116–120
	(Lath)	(Lath)	(Gmass)	(Lath)	(Gmass)	(Large K fsp)	(Gmass)	(Phen core)	(Phen core)	(Mega core)	(Phen core)
SiO_2	50.29	50.71	64.07	51.49	51.58	65.11	54.14	49.39	51.35	48.84	50.40
Al_2O_3	30.61	30.48	18.77	29.60	29.47	18.28	27.81	31.08	29.76	31.75	31.03
Fe_2O_3	0.66	0.65	0.13	0.72	0.90	0.08	1.28	0.88	0.74	0.72	0.54
MnO	0.06	0.00	0.00	0.09	0.03	0.00	0.11	0.00	0.08	0.00	0.08
MgO	0.12	0.06	0.00	0.10	0.16	0.00	0.11	0.29	0.06	0.24	0.08
CaO	14.76	14.52	0.03	13.77	13.58	0.00	11.70	15.40	13.98	16.23	15.40
Na_2O	2.82	3.02	0.41	3.49	3.87	0.22	4.94	2.71	3.68	2.53	3.08
K_2O	0.38	0.24	15.94	0.51	0.17	16.57	0.22	0.09	0.10	0.03	0.07
Total	99.70	99.68	99.36	99.75	99.96	100.27	100.29	100.31	99.75	100.34	100.67
Si	2.306	2.321	2.979	2.357	2.359	3.004	2.453	2.267	2.349	2.235	2.291
Al	1.654	1.644	1.028	1.596	1.588	0.994	1.485	1.681	1.604	1.712	1.662
Fe^3	0.023	0.022	0.005	0.025	0.031	0.003	0.043	0.030	0.026	0.025	0.018
Mn	0.002	0.000	0.000	0.003	0.001	0.000	0.004	0.000	0.003	0.000	0.003
Mg	0.008	0.004	0.000	0.007	0.011	0.000	0.007	0.020	0.004	0.016	0.005
Ca	0.725	0.712	0.002	0.675	0.665	0.000	0.568	0.757	0.685	0.795	0.750
Na	0.250	0.268	0.037	0.310	0.343	0.020	0.434	0.241	0.326	0.225	0.271
K	0.022	0.014	0.945	0.030	0.010	0.975	0.013	0.006	0.006	0.002	0.004
Total	4.990	4.985	4.996	5.003	5.008	4.996	5.007	5.002	5.003	5.010	5.004
Ab	25.11	26.93	3.77	30.51	33.69	2.00	42.78	24.02	32.06	21.99	26.46
Or	2.20	1.43	96.06	2.95	1.00	98.00	1.26	0.55	0.58	0.19	0.40
An	72.69	71.64	0.17	66.54	65.31	0.00	55.96	75.43	67.37	77.82	73.15

Note: Lath = plagioclase lath, Gmass = groundmass, Large K fsp = large K feldspar, Phen core = phenocryst core, and Mega core = megacryst core.

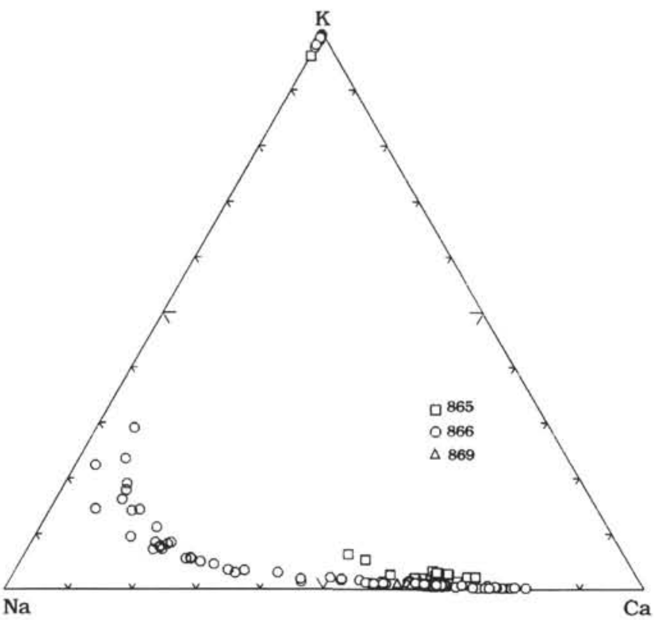

Figure 3. Compositional variations of feldspars from Sites 865 and 866 with Site 869 for comparison.

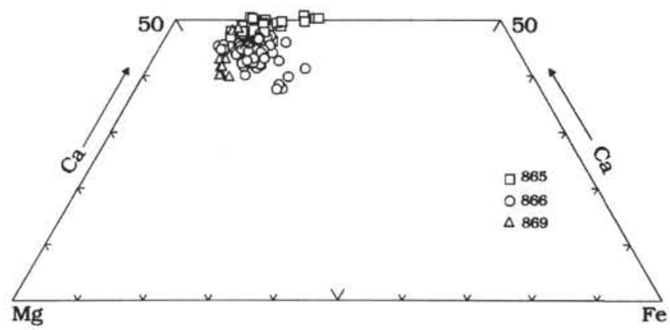

Figure 4. Pyroxene quadrilateral showing compositions of clinopyroxenes from Sites 865 and 866, with samples from Site 869 for comparison.

Geochemistry

Representative whole-rock X-ray fluorescence (XRF) analyses for major and trace elements are presented in Table 6. Except for some pieces of slightly altered basalts from Core 143-866A-177B, all of the volcanic rocks have been moderately to completely altered, mainly to clay minerals. Thus, little significance can be attached to the present concentrations of the more mobile elements (e.g., K_2O, Na_2O). However, plots of major oxides vs. stratigraphic height in the volcanic succession reveal broad compositional changes that are probably insensitive to finer-scale variations caused by alteration. In a plot of MgO vs. depth (Fig. 6A), the only clear distinction is between a group of MgO-rich lavas below 1730 mbsf and generally less magnesian lavas higher up the succession. The more magnesian lavas coincide with those identified as the olivine-phyric group of Unit 12, and the most magnesian of the remainder is equivalent to the thin olivine-phyric Unit 5. A cluster of relatively low-MgO, more differentiated lavas occurs in the middle part of the succession (1690–1710 mbsf). In terms of Al_2O_3 vs. depth (Fig. 6B), this also distinguishes an Al_2O_3-depleted group, corresponding to the Unit 12 olivine-phyric lavas, and a cluster of Al_2O_3-enriched lavas (17%–18% Al_2O_3), corresponding to the plagioclase-phyric suite of Unit 6. A plot of Fe_2O_3/MgO vs. depth (Fig. 6C) separates the lowermost group (Unit 12) from the rest as having lower Fe/Mg ratios. From 1710 mbsf upward, there is a general, though not sharply defined, shift from higher to lower Fe/Mg ratios.

Studies of the alteration of submarine lavas (e.g., Cann, 1970; Hart et al., 1974) have shown that elements such as Ti, Zr, Nb, Y, and most of the REE are not strongly affected during seawater alteration of basalt. In a plot of TiO_2 vs. depth (Fig. 7A) three major geochemical groups are apparent: the Unit 12 lavas with low TiO_2, the Units 8–11 group with high TiO_2, and a later group, above 1673 mbsf, which again has lower TiO_2 but indicates a trend toward higher concentrations with decreasing depth. However, it is plots of Zr, Nb, and REE that are the most illuminating. A plot of Nb/Zr vs. depth (Fig. 7B) distinguishes the uppermost plagioclase-phyric lavas from Unit 6 from the rest of the lavas, because these samples are displaced to lower (0.13–0.15) Nb/Zr ratios. The olivine-phyric lavas from Units 5 and 10 and the lowermost portion of Unit 12 have intermediate

Table 1 (continued).

866A-179R-5	866A-177B-1	866A-177B-1
51–59	1–3	1–3
(Phen core)	(Phen core)	(Lath)
48.54	51.06	56.72
30.95	29.38	26.13
0.66	0.92	0.62
0.10	0.14	0.03
0.11	0.19	0.11
15.95	14.39	9.60
2.82	3.65	6.12
0.06	0.13	0.26
99.18	99.85	99.59
2.249	2.340	2.565
1.691	1.587	1.393
0.023	0.032	0.021
0.004	0.006	0.001
0.007	0.013	0.008
0.792	0.707	0.465
0.254	0.324	0.536
0.003	0.007	0.015
5.023	5.016	5.004
24.18	31.23	52.76
0.32	0.71	1.47
75.50	68.06	45.77

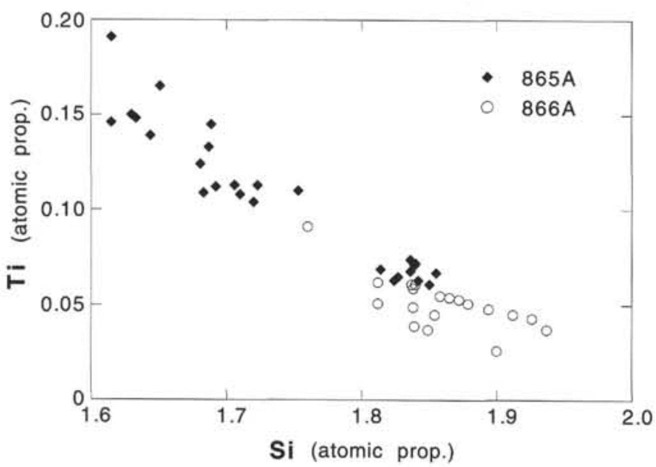

Figure 5. Ti vs. Si (cation proportions on basis of 6 oxygens) in clinopyroxenes from Holes 865A and 866A.

(0.15–0.18) Nb/Zr ratios, whereas the remainder of the volcanic succession, consisting of Units 7, 8, 9, and 11 as well as the upper portion of Unit 12, has high (0.19–0.22) Nb/Zr ratios.

Chondrite-normalized patterns and total concentrations of REE (Fig. 8A) reinforce the three-fold subdivision of the lavas drawn from the ratio of immobile incompatible elements Nb and Zr. The REE contents of the low Nb/Zr basalts from the uppermost part of the succession (i.e., above 1673 mbsf) are only 8 to 60 times chondritic values. More importantly, they have flattened light REE patterns. The relative enrichment of the light to middle REE, represented by La/Sm ratio, for these uppermost basalts is low (~1.4–1.8; Fig. 7C). Conversely, the REE contents of the high Nb/Zr basalts from the middle and lower portions of the succession are 10 to 130 times chondritic values. These samples also are enriched in light REE, having high (~2.4–2.9) La/Sm ratios. Lavas with intermediate Nb/Zr ratios from the middle to lower portions of the Hole 866A basement have 10 to 90 times chondritic values in their REE contents; these lavas are only moderately enriched in light REE (La/Sm ~0.15–0.18). It is important to note, however, that the intermediate group generally overlaps with both the low and high Nb/Zr groups, but more so with the former in

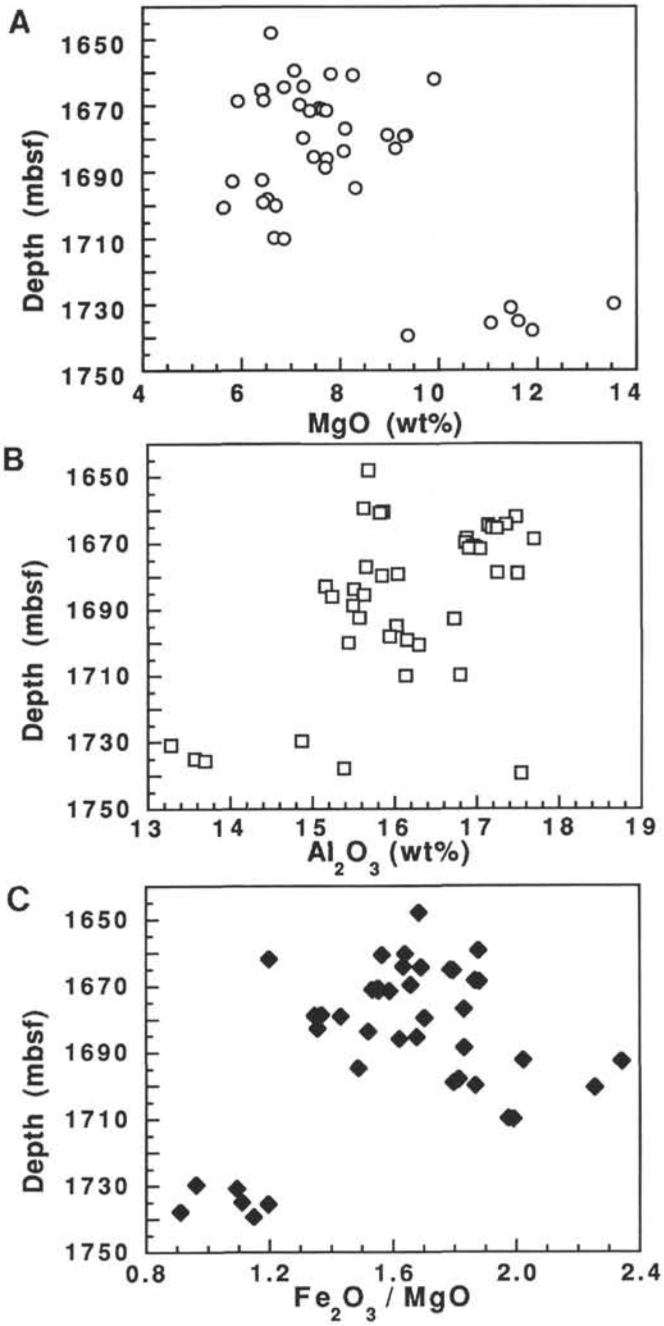

Figure 6. **A.** Concentration of MgO with depth in the volcanic rocks of Hole 866A. Note the more magnesian lavas below 1730 mbsf and the cluster of more differentiated, low-MgO flows, around 1700 mbsf. **B.** Concentration of Al_2O_3 with depth in the volcanic rocks of Hole 866A. **C.** Plot of Fe_2O_3/MgO (atomic) vs. depth in the volcanic rocks of Hole 866A.

terms of concentrations and light-REE enrichment. Specifically, the Unit 5 lavas belong to the less light REE-enriched group despite their intermediate Nb/Zr ratios. The three-fold subdivision of Site 866 samples into low Nb/Zr, high Nb/Zr, and intermediate Nb/Zr geochemical lava groups, as well as the conflicting behavior of the latter group, are clearly shown in a plot of La/Sm vs. Nb/Zr ratios (Fig. 9).

Plots of Nb and Zr vs. TiO_2 (Figs. 10A and 10B) also clearly separate the low Nb/Zr and high Nb/Zr Site 866 lavas, which are also evident in Figure 11. The plagioclase phyric lavas from above 1673 mbsf contain lower Nb and Zr for given TiO_2 than do the plagioclase-olivine-phyric basalts from below 1673 mbsf. The intermediate

Table 2. Representative microprobe analyses (wt% oxide) and atomic proportions of olivines from basaltic rocks in Hole 866A.

Core, section:	189R-1	189R-1	182R-3	182R-3	182R-3	182R-1	182R-1	180R-4	180R-4	180R-3	180R-3
Interval (cm):	66–69	66–69	48–51	48–51	48–51	102–105	102–105	1–4	1–4	116–120	116–120
	(Phen core)	(Large unzoned)	(Phen relict)	(Phen rim)	(Mega core)	(Phen core)	(Phen rim)	(Phen core)	(Phen rim)	(Phen core)	(Phen rim)
SiO_2	39.70	38.46	39.43	38.08	39.18	40.92	38.73	39.84	37.23	40.45	37.35
TiO_2	0.01	0.04	0.07	0.02	0.05	0.01	0.05	0.06	0.05	0.05	0.09
Al_2O_3	0.06	0.04	0.04	0.04	0.03	0.09	0.06	0.08	0.04	0.05	0.03
FeO	15.36	21.39	18.48	23.80	19.85	13.42	23.54	17.04	28.56	13.32	30.76
MnO	0.22	0.28	0.19	0.41	0.35	0.09	0.32	0.28	0.41	0.22	0.46
MgO	43.59	39.03	41.11	36.12	40.35	45.22	37.27	42.26	32.58	45.55	32.18
CaO	0.29	0.26	0.27	0.33	0.27	0.24	0.26	0.28	0.41	0.25	0.35
NiO	0.24	0.11	0.13	0.12	0.19	0.34	0.22	0.28	0.10	0.33	0.17
Total	99.47	99.61	99.72	98.91	100.26	100.33	100.46	100.12	99.37	100.22	101.38
Si	1.005	1.001	1.009	1.010	1.005	1.015	1.009	1.009	1.007	1.006	1.000
Ti	0.000	0.001	0.001	0.000	0.001	0.000	0.001	0.001	0.001	0.001	0.002
Al	0.002	0.001	0.001	0.001	0.001	0.003	0.002	0.002	0.001	0.002	0.001
Fe^2	0.325	0.466	0.395	0.528	0.426	0.278	0.513	0.361	0.646	0.277	0.689
Mn	0.005	0.006	0.004	0.009	0.008	0.002	0.007	0.006	0.009	0.005	0.010
Mg	1.645	1.514	1.568	1.428	1.542	1.672	1.447	1.596	1.313	1.689	1.284
Ca	0.008	0.007	0.008	0.009	0.008	0.006	0.007	0.008	0.012	0.007	0.010
Ni	0.005	0.002	0.003	0.003	0.004	0.007	0.005	0.006	0.002	0.007	0.004
Total	2.995	2.998	2.989	2.988	2.995	2.983	2.991	2.989	2.991	2.994	3.000
Fo	83.3	76.2	79.7	72.7	78.1	85.7	73.6	81.3	66.7	85.7	64.7

Note: Phen core = phenocryst core, Phen relict = phenocryst relict, Phen rim = phenocryst rim, and Mega core = megacryst core.

Table 3. Representative microprobe analyses (wt% oxide) and atomic proportions of clinopyroxenes from basaltic rocks in Hole 866A.

Core, section:	189R-1	186R-3	186R-3	186R-3	185R-3	185R-3	182R-1	181R-3	180R-4	180R-3
Interval (cm):	66–69	12–15	12–15	12–15	88–92	88–92	102–105	91–96	1–4	116–20
	(Gmass)	(Mega core)	(Mega rim)	(Gmass)	(Megacryst)	(Mega rim)	(Phen core)	(Small cryst)	(Small cryst)	(Gmass)
SiO_2	50.62	50.32	49.84	49.30	49.51	50.51	49.44	46.62	50.80	50.28
TiO_2	1.14	0.91	0.97	2.12	1.65	1.21	2.15	3.11	1.57	1.66
Al_2O_3	2.89	4.94	4.77	3.30	3.63	2.85	2.86	5.38	2.19	3.30
Cr_2O_3	0.54	0.52	0.67	0.00	0.04	0.02	0.05	0.11	0.02	0.05
Fe_2O_3	2.04	1.93	2.49	3.51	2.58	2.29	1.72	3.92	1.99	2.31
FeO	5.43	4.46	3.71	5.99	6.76	6.93	10.16	7.07	7.06	6.34
MnO	0.19	0.09	0.10	0.24	0.20	0.32	0.31	0.26	0.27	0.26
MgO	15.09	15.45	15.67	14.69	14.44	14.77	12.76	12.65	14.05	14.07
CaO	21.25	21.32	21.16	20.52	20.47	20.26	19.96	20.28	21.48	21.54
Na_2O	0.39	0.35	0.35	0.46	0.38	0.42	0.49	0.58	0.49	0.51
Total	99.58	100.28	99.73	100.13	99.66	99.58	99.89	99.97	99.90	100.31
Si	1.882	1.846	1.838	1.836	1.851	1.886	1.868	1.756	1.897	1.867
Ti	0.032	0.025	0.027	0.059	0.046	0.034	0.061	0.088	0.044	0.046
Al	0.127	0.214	0.207	0.145	0.160	0.126	0.127	0.239	0.096	0.144
Cr	0.016	0.015	0.019	0.000	0.001	0.001	0.002	0.003	0.001	0.001
Fe^3	0.057	0.053	0.069	0.098	0.073	0.064	0.049	0.111	0.056	0.064
Fe^2	0.169	0.137	0.114	0.186	0.211	0.216	0.321	0.223	0.220	0.197
Mn	0.006	0.003	0.003	0.008	0.006	0.010	0.010	0.008	0.008	0.008
Mg	0.837	0.845	0.861	0.816	0.804	0.822	0.719	0.710	0.782	0.779
Ca	0.847	0.838	0.836	0.819	0.820	0.811	0.808	0.819	0.859	0.857
Na	0.028	0.025	0.025	0.034	0.028	0.031	0.036	0.042	0.035	0.036
Total	4.001	4.001	3.999	4.001	4.000	4.001	4.001	3.999	3.998	3.999
Ca	44.21	44.68	44.38	42.49	42.82	42.15	42.38	43.74	44.62	44.97
Mg	43.68	45.04	45.72	42.33	42.03	42.74	37.69	37.96	40.59	40.88
Fe (+ Mn)	12.10	10.28	9.91	15.18	15.15	15.11	19.93	18.29	14.79	14.15

Note: Gmass = groundmass, Mega core = megacryst core, Mega rim = megacryst rim, Phen core = phenocryst core, and Microphen = microphenocryst.

Nb/Zr lavas surprisingly contain approximately constant Nb and Zr for any given TiO_2. An interesting feature shown by the high Nb/Zr lava group is that it displays a subtle, but nevertheless consistent, chemostratigraphy. The general trend is from lower to higher and then back to lower Nb/TiO_2 ratios upward through the succession, with the maximum value occurring at ~1700 mbsf. This trend also is clearly shown by the Nb/Zr and La/Sm ratios (Figs. 7B and 7C). Higher Nb/TiO_2, Nb/Zr, and La/Sm ratios are associated with more alkalic rocks; thus, the progression is from the mildly alkalic compositions at the bottom of Hole 866A to more alkalic in the middle, and finally to more tholeiitic lavas higher up. The REE-concentration patterns of Site 866 lavas (Fig. 8A) reinforce this notion.

SITE 865

A series of basaltic sills is intrusive into Albian clayey dolomitic limestones between 830 and 870 mbsf in Hole 865A. Two whole-rock K/Ar dates were determined on the sill rocks. The upper (Sample 143-865A-93R, 13–17 cm) gave an age of 87 ± 3 Ma, and the second (Sample 143-865A-93R-4, 78–80 cm), 10 m lower, an age of 102 ± 6 Ma (Pringle et al., this volume). $^{40}Ar/^{39}Ar$ dates by the same authors yield an age of 111.1 ± 2.6 Ma.

Several lines of evidence suggest that the sills were injected into unconsolidated sediments. For example, at the top of Unit 1 (Fig. 12) the overlying soft and muddy sediment becomes increasingly well indurated toward the contact. The actual contact between the basalt and the sediment is irregular and, in some places, is almost vertical, rather than horizontal (Sager, Winterer, Firth, et al., 1993, p. 149, fig. 33). Detached pieces of the clayey bioclastic limestone are included within the basalt, indicating that the latter is younger. Also, there is usually a reaction halo in the basalt where it comes in contact with the sediment, presumably the result of hydrothermal alteration during devolatilization of the wet host material. In some places (e.g., the top of Unit 4), the basalt is clearly chilled against the clayey limestone. In

Table 2 (continued).

177B-1 1–3 (Phen core)	177B-1 1–3 (Phen rim)	177B-1 1–3 (Matrix)
40.83	38.70	37.69
0.00	0.03	0.03
0.07	0.05	0.06
12.54	21.98	24.86
0.00	0.37	0.41
46.07	38.34	36.22
0.28	0.28	0.35
0.19	0.06	0.12
99.97	99.80	99.75
1.012	1.007	0.998
0.002	0.001	0.001
0.260	0.002	0.002
0.000	0.478	0.550
1.702	0.008	0.009
0.007	1.487	1.429
0.004	0.008	0.010
0.000	0.001	0.003
2.987	2.992	3.002
86.7	75.4	71.9

Table 3 (continued).

180R-1 96–100 (Gmass)	179R-5 131–135 (Gmass)	179R-5 51–59 (Gmass)	177B-1 1–3 (Microphen)
49.04	50.74	51.14	50.19
2.16	1.71	1.79	1.62
4.04	2.24	2.42	3.08
0.08	0.05	0.00	0.21
1.86	1.93	1.31	1.93
6.69	7.30	7.18	5.99
0.22	0.16	0.18	0.22
13.50	13.96	14.08	14.46
21.40	21.46	21.63	21.80
0.47	0.51	0.56	0.34
99.46	100.05	100.27	99.83
1.840	1.894	1.899	1.869
0.061	0.048	0.050	0.045
0.179	0.098	0.106	0.135
0.002	0.001	0.000	0.006
0.052	0.054	0.036	0.054
0.210	0.228	0.223	0.187
0.007	0.005	0.006	0.007
0.755	0.777	0.779	0.803
0.860	0.858	0.861	0.870
0.034	0.037	0.040	0.024
4.000	4.000	4.000	4.000
45.65	44.65	45.19	45.31
40.06	40.41	40.91	41.81
14.30	14.95	13.91	12.88

the interior of the basalt, dark reddish brown sedimentary xenoliths are completely decarbonated.

Petrography and Mineralogy

The basaltic sills are highly altered, and few of the original mineral constituents remain unaffected. There are almost certainly oxidized pseudomorphs after olivine in some specimens (e.g., Sample 143-865A-93R-3, 13–17 cm), but there is no fresh relict olivine. Clinopyroxene occurs as a common groundmass constituent and is fairly well preserved. The clinopyroxenes have relatively high Ca in comparison with those from Hole 866A (Fig. 4 and Tables 3 and 4): they range in composition from $Ca_{48}Mg_{43}Fe_9$ to $Ca_{50}Mg_{28}Fe_{22}$ and are commonly zoned. Much of the feldspar is probably primary, and laths show a compositional spread from An_{72} to An_{51}. However, some of the interstitial feldspar is secondary (e.g., the alkali feldspar [$Or_{96}Ab_4$] in Sample 143-865A-93R-3, 13–17 cm). Opaque oxides show a variety of textural forms, some suggestive of rapid cooling.

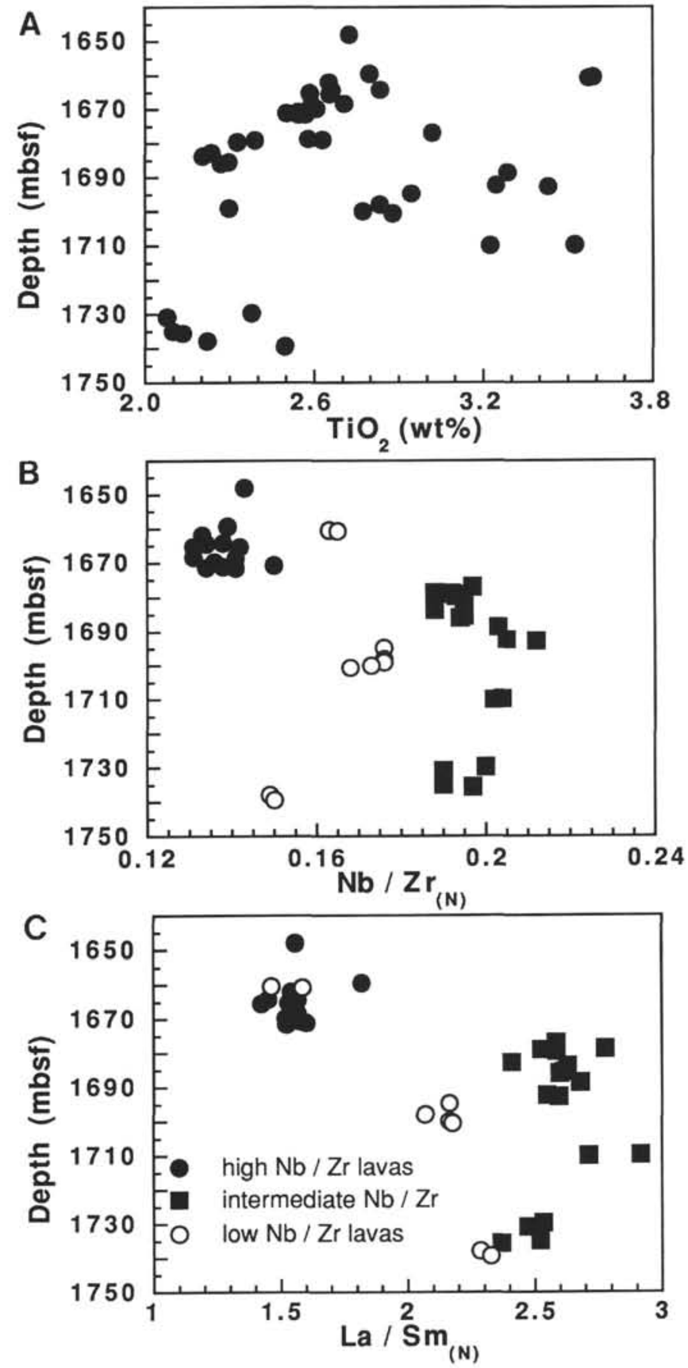

Figure 7. **A.** Plot of TiO_2 vs. depth in Hole 866A. **B.** Plot of Nb/Zr vs. depth in Hole 866A. **C.** Plot of La/Sm vs. depth in Hole 866A. In **B** and **C**, solid circles represent a high Nb/Zr group, solid squares an intermediate Nb/Zr group, and open circles a low Nb/Zr group.

Compositionally, they range from titanomagnetite to ilmenite (e.g., Sample 143-865A-94R-4, 78–80 cm), and there are also some chrome spinels (e.g., Sample 143-865A-93R-3, 13–17 cm).

Geochemistry

The sills are of basaltic composition, but are so highly altered that, again, little reliance can be placed on concentrations of the more mobile elements. XRF whole-rock analyses of a selection of samples from the sills are given in Table 7. The plot of total alkalis (Na_2O +

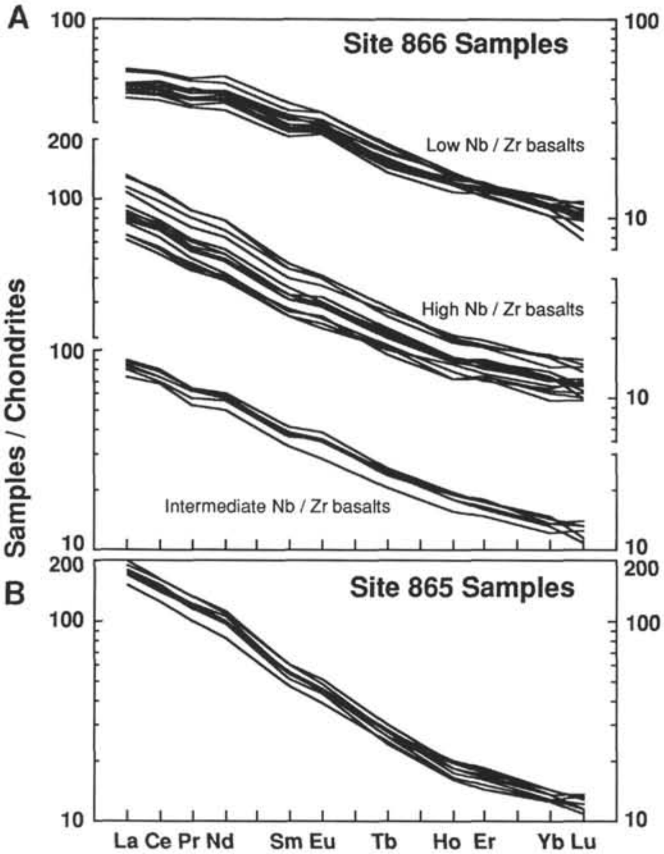

Figure 8. Chondrite-normalized REE patterns for groups of lavas from Hole 866A (**A**) and the basaltic sills of Hole 865A (**B**).

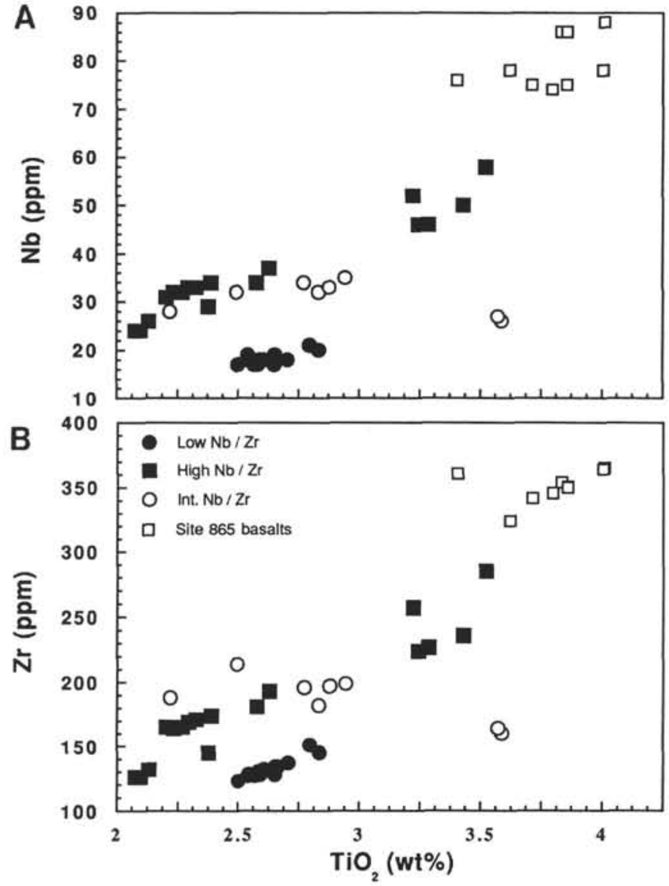

Figure 10. **A.** Plot of Nb vs. TiO_2 for lavas of Hole 866A and the Hole 865A sills. **B.** Plot of Zr vs. TiO_2 for Hole 865A sills and the lavas of Hole 866A.

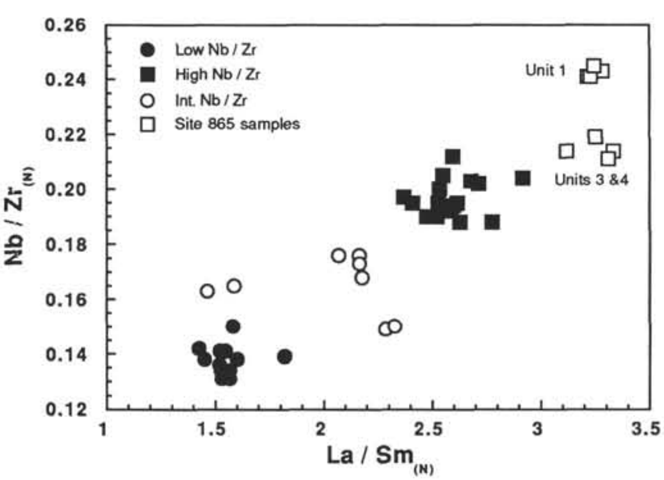

Figure 9. Plot of Nb/Zr vs. La/Sm for the volcanic rocks of Hole 866A.

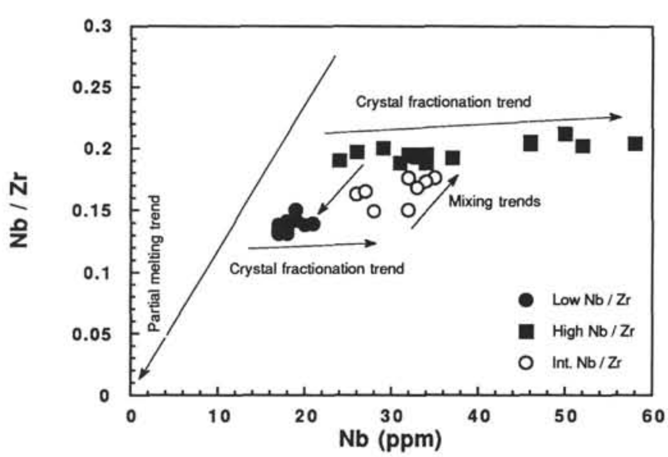

Figure 11. Plot of Nb/Zr vs. Nb for the volcanic rocks of Hole 866A.

K_2O) vs. SiO_2 (Fig. 13) suggests that Site 865 basalts are generally more alkalic than the Site 866 basalts, but little significance can be attached to this in view of the alteration. However, chondrite-normalized REE patterns of Site 865 basalts (Fig. 8B) are steep and more enriched in light REEs than those of the Site 866 lavas. In fact, chondrite-normalized trace element patterns (Fig. 14) point to greater enrichment in incompatible elements in Site 865 basalts compared with the both the Site 866 and Site 869 basalts. Although this must be treated with reservation because of the alteration, comparisons of such elements suggest that Site 865 basalts are more alkalic in composition than any of the other igneous rocks drilled during Leg 143. Of more significance are the consistently higher concentrations and ratios of the alteration-resistant incompatible elements (Nb, Zr, Ti, La, and Sm) in the Site 865 rocks. Plots of Nb/Zr vs. La/Sm (Fig. 9), Nb vs. TiO_2 (Fig. 10A), and Zr vs. TiO_2 (Fig. 10B) illustrate the lack of overlap between basalts from the two sites and show that the Site 865 basalts have generally higher Nb/Zr, Nb/TiO_2, and Zr/TiO_2 ratios. The trace element signature of the Site 865 basalts is typical of highly alkalic or nephelinitic rock suites.

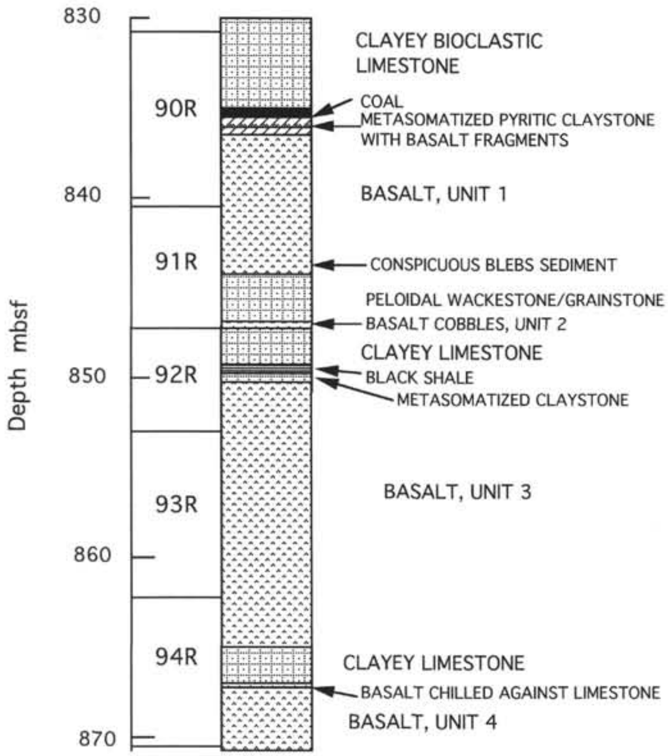

Figure 12. Simplified stratigraphic section through the basaltic sills and their host rocks, 830–870 mbsf, Allison Guyot (Hole 865A).

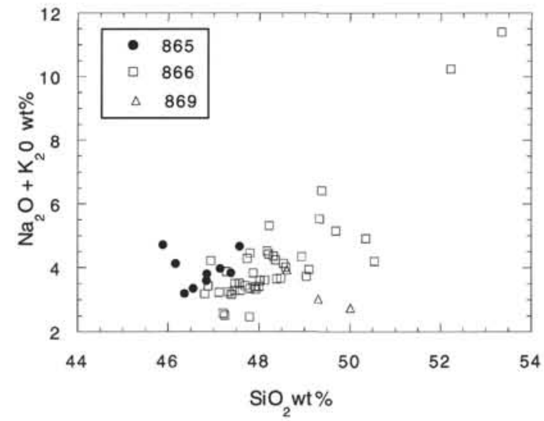

Figure 13. Total alkalis (Na_2O + K_2O) vs. silica plotted for basaltic rocks of Sites 865, 866, and 869.

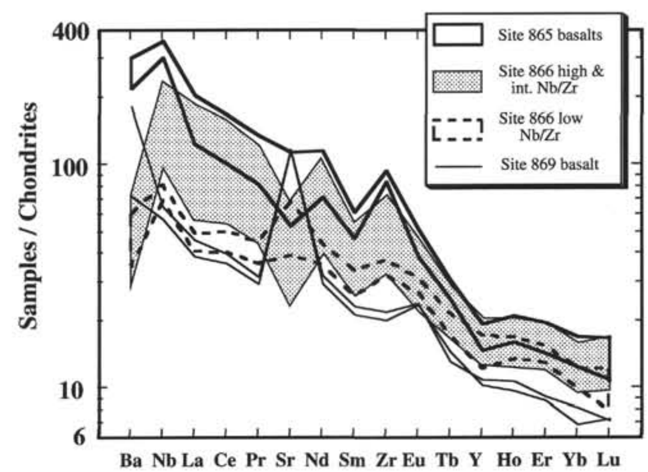

Figure 14. Comparative chondrite-normalized trace-element patterns for basalts from Sites 865, 866, and 869.

Site 865 samples show a slight increase in La/Sm ratios with depth (Fig. 15A,) except for the two samples just below the sedimentary horizon located at the bottom of Section 143-865A-91R-3 to the top of Section 143-865A-92R-3 (i.e., samples from the top of Unit 3); these two samples have the lowest La/Sm ratios of all. Basalts from the thin (~15 cm.) Unit 2, which are apparently interbedded with the sediments, were not analyzed because these samples are extremely altered. It was noted before, however, that Unit 2 could have been composed of cobbles from Unit 1, because they lie on top of Section 143-865A-92R (Sager, Winterer, Firth, et al., 1993). Interestingly, all Units 3 and 4 samples have similar and low Nb/Zr ratios (0.21–0.22) that are clearly distinct from the Nb/Zr ratios (0.24–0.25) of Unit 1 samples above the sediments (Figs. 9 and 15B). Unit 1 basalts also have generally higher Nb/TiO_2 ratios than Units 3 and 4 basalts (Fig. 10A). In summary, therefore, the general trend of Site 865 basalts is toward less alkalic composition with depth.

PETROGENESIS

The similar ratios of alteration-resistant trace elements of the geochemically enriched (i.e., high Nb/Zr ratio) Site 866 lavas clearly suggest that samples belonging to the group are petrogenetically related through a simple magmatic differentiation mechanism. The same is true for the geochemically depleted (low Nb/Zr ratio) group. The relationship among the mildly enriched (intermediate Nb/Zr) lavas is probably more complex because their geochemical characteristics overlap with both the depleted and the enriched groups. Because of the altered state of the majority of the lavas, it is difficult to evaluate quantitatively the main differentiation mechanism or mechanisms that relate samples within and between the geochemical groups. However, a plot of a ratio of two highly incompatible trace elements vs. the concentration of one of those elements can identify semiquantitatively such mechanisms (e.g., Minster and Allegré, 1978). Figure 11, a plot of Nb/Zr ratios vs. Nb, shows that the enriched and depleted Site 866 lavas define crystal fractionation trends. Figure 11 also shows it is highly unlikely that the mildly enriched lavas have their own crystal fractionation trend; rather, the lavas are probably the products of mixing between the first and second groups.

To test the crystal fractionation hypothesis for Site 866 lavas further, the major element contents of the least-altered samples, based on petrography and low LOI contents, were modeled through the least-squares mixing program (Le Maitre, 1980) and using mineral analyses actually present in these rocks (Tables 1–5) as the fractionating phases. Two methods were employed: (1) the incremental step method, in which each differentiated rock was modeled by subtracting an appropriate combination of minerals from a slightly more mafic rock and so on until the most differentiated rock was produced and (2) the cumulative step method, in which all differentiated rocks were modeled from a single most mafic magma. Representative results of the modeling are shown in Table 8. Basically, models involving samples that have similar Nb/Zr ratios (i.e., models between samples from within the depleted and the enriched group) produce acceptable results. The residual sum of squares of the difference in the major element contents of the actual parental rock and the parental magma predicted by the model ($\sum r_i 2$) are generally <<0.1, except in models involving more differentiated samples, and the kind and proportion of minerals re-

Table 4. Representative microprobe analyses (wt% oxide) and atomic proportions of clinopyroxenes from basaltic rocks in Hole 865A. All are small grains in range 0.02–0.2 mm.

Core, section:	94R-4	94R-4	94R-4	93R-3	93R-3	93R-3	93R-3	93R-3	93R-3	93R-3	91R-1
Interval (cm):	78–80	78–80	78–80	13–17	13–17	13–17	13–17	13–17	13–17	13–17	128–130
SiO_2	44.93	43.44	42.22	49.59	48.65	45.31	44.89	44.57	42.24	42.24	49.01
TiO_2	4.70	5.76	6.64	2.27	2.45	3.99	3.97	4.36	5.08	5.17	2.33
Al_2O_3	7.47	7.87	8.17	4.11	4.12	7.19	7.16	7.32	8.46	8.23	4.07
Cr_2O_3	0.03	0.07	0.00	0.27	0.00	0.14	0.00	0.06	0.00	0.00	0.28
Fe_2O_3	2.27	2.12	2.36	0.97	3.07	2.39	3.86	3.57	5.04	4.12	2.01
FeO	5.82	6.89	7.09	4.80	4.38	4.86	4.08	5.35	6.61	8.33	4.25
MnO	0.12	0.09	0.20	0.05	0.14	0.13	0.21	0.26	0.17	0.18	0.04
MgO	11.92	10.94	10.43	14.47	13.85	12.39	12.03	11.72	9.70	8.71	14.68
CaO	22.26	21.60	21.47	22.62	22.72	22.54	22.84	22.13	21.88	21.70	22.18
Na_2O	0.49	0.64	0.66	0.37	0.44	0.39	0.48	0.51	0.64	0.72	0.40
Total	100.00	99.41	99.25	99.51	99.83	99.32	99.53	99.85	99.83	99.40	99.24
Si	1.687	1.651	1.615	1.842	1.814	1.706	1.692	1.681	1.615	1.630	1.827
Ti	0.133	0.165	0.191	0.063	0.069	0.113	0.112	0.124	0.146	0.150	0.065
Al	0.331	0.352	0.369	0.180	0.181	0.319	0.318	0.326	0.381	0.374	0.179
Cr	0.001	0.002	0.000	0.008	0.000	0.004	0.000	0.002	0.000	0.000	0.008
Fe^3	0.064	0.061	0.068	0.027	0.086	0.068	0.109	0.101	0.145	0.120	0.056
Fe^2	0.183	0.219	0.227	0.149	0.137	0.153	0.129	0.169	0.211	0.269	0.132
Mn	0.004	0.003	0.006	0.001	0.004	0.004	0.007	0.008	0.005	0.006	0.001
Mg	0.667	0.620	0.595	0.801	0.770	0.695	0.676	0.659	0.552	0.501	0.816
Ca	0.895	0.880	0.880	0.901	0.908	0.909	0.922	0.894	0.896	0.897	0.886
Na	0.036	0.047	0.049	0.027	0.032	0.028	0.035	0.037	0.048	0.054	0.029
Ca	49.39	49.35	49.55	47.91	47.66	49.71	50.05	48.83	49.5	50.06	46.84
Mg	36.79	34.78	33.48	42.64	40.41	38.01	36.67	35.97	30.52	27.94	43.12
Fe (+ Mn)	13.82	15.86	16.97	9.45	11.93	12.28	13.27	15.2	19.98	22.00	10.04

Note: All analyses are small grains ranging from 0.02 to 0.2 mm.

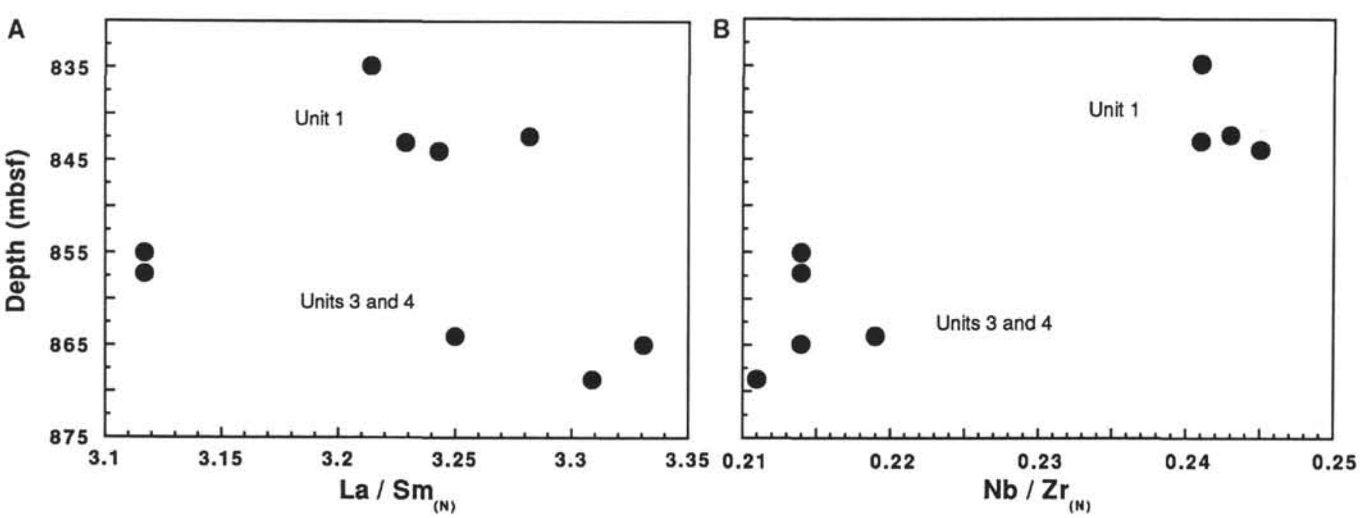

Figure 15. Plots of La/Sm (**A**) and Nb/Zr (**B**) vs. depth in Hole 865A.

moved from the parental magma are those actually present in the parental magma. Model results for samples belonging to the mildly enriched group also produce acceptable results, but only for the incremental step method because the more mafic lavas of this group have high LOI and K_2O contents (e.g., Samples 143-866A-189R-3, 2–4 cm, and -189R-4, 11–14 cm). Surprisingly, cumulative step results between mafic depleted basalts and differentiated mildly alkalic lavas are also acceptable. Other intragroup models produce unreasonable results.

The Site 865 basalts are more difficult to evaluate for crystal fractionation because, in addition to having fewer samples, they are generally more altered than Site 866 basalts. Specifically, the more mafic basalts have high K_2O (and LOI) values so that results of cumulative models are unreasonable. Incremental model results for the differentiated basalts from Units 3 and 4 are reasonable.

In summary, major-element modeling results are consistent with the crystal fractionation origin of the intergroup Nb variations, shown by Site 866 depleted and enriched lavas. Modeling results for the mildly enriched lavas suggest that these rocks are possibly related through crystal fractionation, but most probably are also affected to a large extent by mixing between geochemically depleted and enriched magmas. The intermediate behavior of the trace-element contents of the mildly enriched group, between the enriched and the depleted group (e.g., Figs. 7–10), is also consistent with this mixing scenario. The geochemical variations of Site 865 basalts are subject to greater uncertainty because of alteration, but some may be attributable to simple crystal fractionation.

The above interpretations are consistent with the Sr, Nd, and Pb isotopic ratios of the samples (P.R. Castillo et al., unpubl. data), particularly those for the Site 866 lavas. The Pb and Sr isotopic ratios of the enriched basalts from Site 866 are generally higher than those of the depleted basalts; the Sr and Pb isotopic ratios of the mildly enriched group lie between the first two groups, supporting the suggestion from major- and trace-element data that they are likely to be mixing products. Site 865 basalts exhibit a range of isotopic values, but these do not show any systematic difference between the less alkalic Units 3 and 4 and the more alkalic Unit 1.

Table 4 (continued).

91R-1	91R-1	91R-1
128–130	128–130	128–130
49.52	49.19	45.31
2.43	2.51	3.64
4.45	4.49	6.92
0.28	0.21	0.01
0.63	0.00	2.84
6.12	6.96	5.47
0.12	0.15	0.08
13.73	13.67	11.77
22.51	21.96	22.20
0.40	0.31	0.54
100.20	99.45	98.79
1.836	1.839	1.720
0.068	0.071	0.104
0.195	0.198	0.310
0.008	0.006	0.000
0.018	0.000	0.081
0.190	0.218	0.174
0.004	0.005	0.003
0.759	0.761	0.666
0.894	0.880	0.903
0.028	0.022	0.039
47.97	47.21	49.42
40.70	40.86	36.47
11.33	11.93	14.11

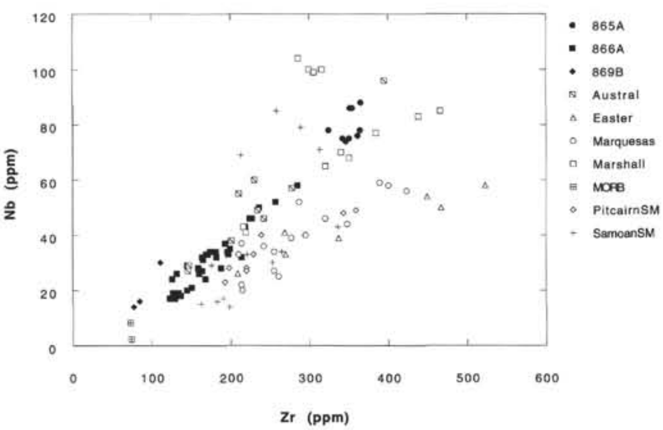

Figure 16. Plot of Nb vs. Zr for basaltic rocks of the Leg 143 sites, compared with lavas from other South Pacific seamounts and archipelagos. Sources of data as follows: Austral (Palacz and Saunders, 1986); Easter (Baker et. al., 1974); Marquesas (Woodhead, 1992); Marshall (Davis et al., 1989); MORB (Sun and McDonough, 1989); Pitcairn seamounts (Woodhead and Devey, 1993); Samoan seamounts (Johnson et al., 1986).

DISCUSSION

The basement of Site 866 was originally considered to be a sequence of subaerial lava flows with interbasaltic intervals (Sager, Winterer, Firth, et al., 1993). The latter were of various types, interpreted as rubbly aa, scoriaceous talus, debris flows, or boles. However, neither the radiometric dating (Pringle et al., this volume) nor the geochemical variations support this contention. Deviations from a systematic progression may be explained by the occurrence of intrusives within the lava pile, although evidence for this remains indirect as no intrusive contacts were recognized in the core.

Fractional crystallization is the dominant magmatic differentiation mechanism responsible for the variation of major- and trace-element contents of samples within different rock groups. These groups are most clearly distinguished on the basis of REE, Nb/Zr, La/Sm, and other trace-element criteria. However, the different groups must have come from different mantle sources, as implied by the geochemical evidence presented here and confirmed by their Sr, Nd, and Pb isotopic compositions (P.R. Castillo et al., unpubl. data).

Allison and Resolution seamounts originated within the region of the South Pacific Isotopic and Thermal Anomaly or SOPITA (Staudigel et al., 1991). SOPITA embraces the area previously designated the South Pacific Superswell (McNutt and Fischer, 1987) and includes a part of the Dupal Anomaly (Hart, 1984). It incorporates a series of island hotspots whose lavas bear the imprint of both HIMU (high U/Pb) and EMII (enriched mantle) source regions, as defined, for example, in Zindler and Hart (1986). The proportions of these components vary across the region, with EMII prevailing in the northern islands (Samoa-Marquesas) and HIMU in the more southerly hotspots, such as the Cook-Austral groups (Staudigel et al., 1991). From their work on Cretaceous seamounts, the same authors established the longevity of the anomaly by demonstrating that isotopically distinctive lavas have been generated at SOPITA for at least 120 m.y. A more recent study by Castillo et al. (1992) pushed the isotopic anomaly even farther back, to ~160 Ma. However, evidence suggests that the degree of enrichment or proportions of mantle components may not have remained constant over this long period of time. For this reason, trace element and isotopic characteristics of Cretaceous seamounts may not necessarily be used to relate them to specific present-day hotspots or island groups within the SOPITA area.

Lineaments derived by backtracking seamounts in the Pacific hotspot reference frame (Duncan and Clague, 1985; Smith et al., 1989) point to an origin of Resolution and Allison seamounts in the vicinity of the Tubuai, Society, or Tuamotu islands. Despite reservations about compositional changes with time, this link is supported by comparative plots of the immobile incompatible elements, such as Nb and Zr (Fig. 16). The Site 865 and 866 sills and lavas are more closely coincident with the Austral Islands lavas than with those of any other group. There is a certain amount of scatter, and the Samoan seamounts (Johnson et al., 1986) separate into trends with both high and low Nb/Zr ratios. However, in general, high Nb/Zr ratios are characteristic of the more westerly islands and lower ratios prevail in the east (Marquesas, Pitcairn seamounts, and Easter Island). Resolution and Allison guyots, together with the Austral Islands, lie both geographically and compositionally in the middle. In a broad sense, the incidence of more extreme alkaline compositions seems to increase toward the west across the SOPITA hotspots and their derivative seamounts. Similar east-west compositional gradations were reported by Palacz and Saunders (1986), who found that westward the islands become more enriched in large ion lithophile elements (LILE) and that they are isotopically enhanced in the Dupal components (high $^{87}Sr/^{86}Sr$, low $^{143}Nd/^{144}Nd$, and low $^{207}Pb/^{206}Pb$).

Judging by their inferred tracks (Duncan and Clague, 1985), the Resolution and Allison seamounts may have followed essentially the same path and, therefore, may have been fed at different times by the same hotspot. The lavas of Resolution Guyot show an upward shift from more alkaline to more tholeiitic compositions, which may reflect an increase in partial melting as the volcano approached and passed over a hotspot. On this basis, the alkaline sills of Allison Guyot may represent residual activity after the seamount had passed over a hotspot. But this scenario seems unlikely because light REE and other incompatible elements are more enriched as well, and the ratios tend to be slightly higher in the Site 865 sills than in the Site 866 lavas. The higher La/Sm and La/Yb ratios in the Site 865 basalts may be indicative of a greater depth of melt segregation. Moreover, the Sr, Nd, and Pb isotopic ratios of Resolution Guyot have more HIMU components than those of Allison (P.R. Castillo et al., unpubl. data). Thus, the compositional variations might be an expression of influx from two mantle components (Palacz and Saunders, 1986) whose relative contributions varied at different hotspots. It is also possible that the guyots each passed over at least two distinct hotspots. In the case of Allison Guyot, where the volcanic basement was not reached during drilling, the sills may represent a later phase of activity unrelated to the main phase of volcanism.

Table 5. Representative microprobe analyses (wt%) and atomic proportions of Fe-Ti oxides and spinels from Hole 866A.

Core, section:	177B-1	177B-1	177B-1	180R-3	181R-3	185R-3	180R-4	171R-3	185R-2	185R-3	189R-1	182R-1
Interval (cm):	1–3	1–3	1–3	116–120	91–96	88–92	1–4	70–73	62–66	88–92	66–69	102–105
	(Spinel)	(Ti-Mt)	(Ti-Mt)	(Ti-Mt)	(Ti-Mt)	(Ti-Mt)	(Ti-Mt)	(Ilmenite)	(Ilmenite)	(Cr-spinel)	(Cr-spinel)	(Ti-Mt)
SiO_2	0.05	0.10	0.05	0.05	0.41	0.09	0.03	0.04	0.01	0.00	0.00	0.00
TiO_2	3.12	16.18	16.52	27.56	13.90	22.89	27.28	49.31	49.77	1.48	0.68	18.47
Al_2O_3	26.01	7.69	7.52	1.14	0.47	2.41	1.32	0.00	0.00	26.20	32.90	8.14
Cr_2O_3	21.48	9.48	8.91	0.19	0.37	5.49	0.13	0.17	0.00	31.35	24.61	1.89
Fe_2O_3	16.58	20.79	20.85	15.29	40.99	15.40	13.88	8.33	6.07	12.27	10.83	43.08
FeO	21.91	39.27	39.84	52.63	39.16	48.55	51.46	36.36	40.48	16.18	19.21	21.61
MnO	0.28	0.42	0.37	0.77	0.47	0.68	0.60	0.67	0.58	0.19	0.25	0.34
MgO	10.86	4.86	4.71	2.21	2.41	1.77	2.37	4.14	2.07	12.84	11.30	6.84
CaO	0.00	0.11	0.11	0.08	0.22	0.09	0.16	0.25	0.03	0.00	0.00	0.00
NiO	0.16	0.05	0.16	0.00	0.03	0.07	0.06	0.00	0.00	0.13	0.23	0.18
ZnO	0.00	0.00	0.00	0.08	0.03	0.19	0.20	0.00	0.00	0.11	0.20	0.01
Total	100.45	98.95	99.03	99.99	98.45	97.62	97.49	99.28	99.00	100.74	100.21	100.54
Si	0.002	0.004	0.002	0.002	0.015	0.003	0.001	0.002	0.000	0.000	0.000	0.000
Ti	0.072	0.429	0.439	0.760	0.393	0.644	0.769	1.835	1.884	0.033	0.015	0.456
Al	0.944	0.320	0.313	0.049	0.021	0.106	0.058	0.000	0.000	0.932	1.157	0.315
Cr	0.523	0.264	0.249	0.005	0.011	0.163	0.004	0.007	0.000	0.748	0.581	0.049
Fe^3	0.384	0.552	0.554	0.422	1.161	0.434	0.392	0.310	0.230	0.279	0.243	1.065
Fe^2	0.564	1.158	1.177	1.613	1.233	1.520	1.613	1.504	1.705	0.408	0.479	0.594
Mn	0.007	0.013	0.011	0.024	0.015	0.022	0.019	0.028	0.025	0.005	0.006	0.009
Mg	0.499	0.255	0.248	0.121	0.135	0.099	0.133	0.306	0.155	0.577	0.502	0.335
Ca	0.000	0.004	0.004	0.003	0.009	0.004	0.006	0.013	0.002	0.000	0.000	0.000
Ni	0.004	0.001	0.004	0.000	0.001	0.002	0.002	0.000	0.000	0.003	0.006	0.005
Zn	0.000	0.000	0.000	0.002	0.001	0.005	0.006	0.000	0.000	0.002	0.004	0.000
Total	2.999	3.000	3.001	3.001	2.995	3.002	3.003	4.005	4.001	2.987	2.993	2.828
Fe number	65.73	87.09	87.54	94.46	94.69	95.24	93.85	85.77	92.67	41.7	49.15	64.31
Cr/Cr + Al	35.65	45.26	44.29	9.95	34.46	60.5	6.24	100	0	44.53	33.42	13.45

Note: Ti-Mt = titanomagnetite.

ACKNOWLEDGMENTS

We thank members of the technical staff of the Department of Earth Sciences, Leeds University, and Scripps Institution of Oceanography for the preparation of thin sections and rock crushing. In particular, we thank Alan Gray for the XRF analyses and Elizabeth Kristofetz for the ICP-MS analyses. Improvements to the manuscript were made on the basis of helpful comments by Andrew Saunders, John Sinton, and Sondra Stewart.

REFERENCES*

Baker, P.E., Buckley, F., and Holland, J.G., 1974. Petrology and geochemistry of Easter Island. *Contrib. Mineral. Petrol.,* 44:85–100.

Cann, J.R., 1970. Rb, Sr, Y, Zr, and Nb in some ocean floor basaltic rocks. *Earth Planet. Sci. Lett.,* 10:7–11.

Castillo, P.R., Floyd, P.A., and France-Lanord, C., 1992. Isotope geochemistry of Leg 129 basalts: implications for the origin of the widespread Cretaceous volcanic event in the Pacific. *In* Larson, R.L., Lancelot, Y., et al., *Proc. ODP, Sci. Results,* 129: College Station, TX (Ocean Drilling Program), 405–413.

Davis, A.S., Pringle, M.S., Pickthorn, L.B.G., Clague, D.A., and Schwab, W.C., 1989. Petrology and age of alkalic lava from the Ratak Chain of the Marshall Islands. *J. Geophys. Res.,* 94:5757–5774.

Duncan, R.A., and Clague, D.A., 1985. Pacific plate motion recorded by linear volcanic chains. *In* Nairn, A.E.M., Stehli, F.G., and Uyeda, S. (Eds.), *The Ocean Basins and Margins* (Vol. 7A): *The Pacific Ocean:* New York (Plenum), 89–121.

Fodor, R.V., Keil, K., and Bunch, T.E., 1975. Contributions to the mineral chemistry of Hawaiian rocks. IV. Pyroxenes in rocks from Haleakala and West Maui volcanoes, Maui, Hawaii. *Contrib. Mineral. Petrol.,* 50:173–195.

*Abbreviations for names of organizations and publications in ODP reference lists follow the style given in *Chemical Abstracts Service Source Index* (published by American Chemical Society).

Harland, W.B., Armstrong, R.L., Cox, A.V., Craig, L.E., Smith, A.G., and Smith, D.G., 1990. *A Geologic Time Scale, 1989:* Cambridge (Cambridge Univ. Press).

Hart, S.R., 1984. A large-scale isotope anomaly in the Southern Hemisphere mantle. *Nature,* 309:753–757.

Hart, S.R., Erlank, A.J., and Kable, E.J.D., 1974. Sea floor basalt alteration: some chemical and Sr isotopic effects. *Contrib. Mineral. Petrol.,* 44:219–230.

Johnson, K.T.M., Sinton, J.M., and Price, R.C., 1986. Petrology of seamounts northwest of Samoa and their relation to Samoan volcanism. *Bull. Volcanol.,* 48:225–235.

Le Bas, M.J., 1962. The role of aluminum in igneous clinopyroxenes with relation to their parentage. *Am. J. Sci.,* 260:267–288.

LeMaitre, R.W., 1980. A generalized petrological mixing model program. *Comput. Geosci.,* 7:229–247.

McNutt, M.K., and Fischer, K.M., 1987. The South Pacific superswell. *In* Keating, B.H., Fryer, P., Batiza, R., and Boehlert, G.W. (Eds.), *Seamounts, Islands, and Atolls.* Geophys. Monogr., Am. Geophys. Union, 43:25–34.

Minster, J.F., and Allegré, C.J., 1978. Systematic use of trace elements in igneous processes. Part III: inverse problem of batch partial melting in volcanic suites. *Contrib. Mineral. Petrol.,* 69:37–52.

Palacz, Z.A., and Saunders, A.D., 1986. Coupled trace element and isotope enrichment in the Cook-Austral-Samoa islands, southwest Pacific. *Earth Planet. Sci. Lett.,* 79:270–280.

Sager, W.W., Winterer, E.L., Firth, J.V., et al., 1993. *Proc. ODP, Init. Repts.,* 143: College Station, TX (Ocean Drilling Program).

Schweitzer, E.L., Papike, J.J., and Bence, A.E., 1979. Statistical analysis of clinopyroxenes from deep-sea basalts. *Am. Mineral.,* 64:501–513.

Shipboard Scientific Party, 1981. Site 463: western Mid-Pacific Mountains. *In* Thiede, J., Vallier, T.L., et al., *Init. Repts. DSDP,* 62: Washington (U.S. Govt. Printing Office), 33–156.

Smith, W.H.F., Staudigel, H., Watts, A.B., and Pringle, M.S., 1989. The Magellan Seamounts: Early Cretaceous record of the South Pacific isotopic and thermal anomaly. *J. Geophys. Res.,* 94:10501–10523.

Staudigel, H., Park, K.-H., Pringle, M., Rubenstone, J.L., Smith, W.H.F., and Zindler, A., 1991. The longevity of the South Pacific isotopic and thermal anomaly. *Earth Planet. Sci. Lett.,* 102:24–44.

Sun, S.-S., and McDonough, W.F., 1989. Chemical and isotopic systematics of oceanic basalts: implications for mantle composition and processes. *In*

Saunders, A.D., and Norry, M.J. (Eds.), *Magmatism in the Ocean Basins.* Geol. Soc. Spec. Publ. London, 42:313–345.

Woodhead, J.D., 1992. Temporal geochemical evolution in oceanic intra-plate volcanics: a case study from the Marquesas (French Polynesia) and comparison with other hot spots. *Contrib. Mineral. Petrol.,* 111:458–467.

Woodhead, J.D., and Devey, C.W., 1993. Geochemistry of the Pitcairn seamounts, I: source character and temporal trends. *Earth and Planet. Sci. Lett.,* 116:81–99.

Zindler, A., and Hart, S., 1986. Chemical geodynamics. *Annu. Rev. Earth Planet. Sci.,* 14:493–571.

Date of initial receipt: 1 December 1993
Date of acceptance: 6 July 1994
Ms 143SR-216

Table 6. Whole-rock XRF and ICP-MS analyses of basaltic lavas from Hole 866A.

Core, section:	171R-3	171R-3	174R-1	177R-1	179R-1	179R-2	179R-2	179R-5	179R-5	179R-5
Interval (cm):	70–73	143–146	3–5	10–13	108–112	13–18	137–140	32–35	51–59	131–135
SiO_2	49.63	50.25	47.05	46.84	45.51	46.87	47.23	46.44	46.62	46.21
TiO_2	2.91	2.77	2.65	2.76	3.42	3.45	2.52	2.75	2.61	2.51
Al_2O_3	17.29	16.31	15.25	15.42	15.12	15.28	16.61	16.84	16.80	16.69
Fe_2O_3	11.50	9.54	10.80	13.11	12.22	12.49	11.29	11.52	11.39	11.16
MnO	0.05	0.08	0.15	0.17	0.25	0.23	0.38	0.24	0.24	0.16
MgO	2.41	1.68	6.41	6.98	7.45	7.98	9.42	7.05	6.73	6.24
CaO	1.22	2.59	11.07	9.66	7.01	6.02	2.48	8.20	9.94	10.71
Na_2O	0.85	0.68	3.00	2.98	3.25	3.26	2.32	3.01	3.03	2.80
K_2O	8.88	10.07	0.55	0.47	0.83	0.75	2.455	0.71	0.41	0.40
P_2O_5	0.28	0.22	0.30	0.29	0.26	0.25	0.21	0.25	0.24	0.24
LOI	5.10	5.97	3.06	1.79	4.56	3.60	5.68	3.16	1.79	2.33
Total	100.12	100.16	100.29	100.472	99.88	100.16	100.72	100.17	99.80	99.45
Rare earth elements (in ppm) by ICP-MS:										
La	11.3	12.2	14.7	14.4	13.6	13.4	9.7	11.4	11.3	10.8
Ce	26.1	25.80	37.2	35.0	34.6	33.5	24.7	29.8	29.0	27.8
Pr	3.52	4.06	5.10	4.65	4.81	4.72	3.43	4.15	4.04	3.81
Nd	17.1	19.2	25.0	22.3	24.0	22.7	16.6	20.3	19.9	18.5
Sm	3.81	4.64	5.93	4.97	5.84	5.30	3.95	4.94	4.55	4.45
Eu	1.25	1.43	1.90	1.83	1.94	1.95	1.54	1.73	1.69	1.60
Tb	0.62	0.70	0.91	0.85	0.90	0.85	0.64	0.80	0.72	0.67
Ho	0.70	0.71	1.06	1.10	0.96	0.91	0.76	0.95	0.89	0.86
Er	1.79	1.73	2.92	2.97	2.45	2.46	2.20	2.42	2.52	2.40
Yb	1.26	1.36	2.45	2.34	2.09	1.91	1.68	1.94	1.97	1.88
Lu	0.16	0.19	0.40	0.35	0.28	0.24	0.25	0.31	0.26	0.26
Other trace elements (in ppm) by XRF:										
Ba	203	254	112	92	109	116	145	99	96	97
Co	47	40	53	54	61	61	53	50	46	48
Cr	594	602	416	176	292	302	207	182	175	162
Cu	37	69	81	76	53	55	120	80	67	77
Nb	22	22	24	21	26	27	17	20	18	17
Ni	386	297	246	135	199	200	137	136	136	131
Rb	59	51	8	5	5	7	16	7	6	5
Sc	29	22	24	24	24	22	29	26	19	14
Sr	63	71	580	396	552	538	283	468	480	495
Th	5	6	7	6	6	6	6	6	8	7
V	151	210	251	306	274	289	300	288	259	241
Y	19	20	27	27	26	25	19	27	24	24
Zn	168	76	100	99	109	111	82	91	84	79
Zr	147	143	168	151	160	164	128	145	134	130

Notes: Major oxides in weight percent (%), and trace elements in parts per million (ppm). LOI = loss on ignition.

Table 6 (continued).

179R-6 10–13	180R-1 96–100	180R-1 132–136	180R-2 102–106	180R-3 79–82	180R-3 116–120	180R-4 1–4	180R-4 7–11	181R-1 121–125	181R-2 144–148
46.94	46.71	47.17	46.41	46.23	46.54	46.01	46.32	46.47	47.26
2.60	2.65	2.54	2.55	2.48	2.47	2.52	2.49	2.84	2.47
16.90	16.53	17.35	16.49	16.54	16.78	16.59	16.68	14.73	16.53
11.28	11.80	10.92	11.64	11.48	11.60	11.78	11.49	13.97	11.75
0.16	0.14	0.16	0.16	0.16	0.16	0.17	0.16	0.19	0.29
6.28	6.32	5.81	7.02	7.39	7.56	7.58	7.23	7.63	8.59
10.24	10.17	10.30	10.07	9.97	10.24	9.88	10.11	1.85	3.31
2.93	2.95	3.03	2.81	2.69	2.82	2.96	2.79	1.61	2.67
0.41	0.42	0.52	0.41	0.39	0.37	0.41	0.38	4.43	2.63
0.24	0.25	0.23	0.23	0.22	0.23	0.24	0.22	0.38	0.31
2.33	2.02	2.20	2.36	1.99	1.62	1.95	1.85	6.32	5.11
100.31	99.96	100.23	100.15	99.54	100.39	100.09	99.72	100.42	100.92
11.6	11.2	10.4	11.6	11.0	11.0	10.7	10.50	22.7	18.7
30.6	28.9	26.6	27.7	27.7	27.7	26.9	26.90	51.7	40.6
4.23	3.89	3.57	4.30	3.76	3.78	3.72	3.57	6.12	4.78
20.6	19.3	18.1	19.4	18.6	19.0	18.6	17.8	26.3	20.2
5.14	4.51	4.21	4.83	4.37	4.34	4.43	4.35	5.54	4.23
1.79	1.65	1.58	1.75	1.60	1.57	1.56	1.60	1.63	1.49
0.80	0.70	0.68	0.69	0.73	0.75	0.68	0.72	0.81	0.62
0.93	0.91	0.85	0.84	0.86	0.83	0.83	0.84	0.99	0.70
2.47	2.55	2.32	2.14	2.33	2.40	2.24	2.34	2.83	2.10
2.06	1.94	1.84	1.71	1.96	1.83	1.93	1.95	2.44	1.59
0.30	0.25	0.22	0.20	0.27	0.26	0.28	0.26	0.35	0.24
90	97	89	87	94	91	93	84	136	122
45	48	45	49	49	45	47	48	61	66
192	173	206	192	192	183	167	187	402	455
71	101	98	70	71	79	76	75	79	75
19	18	18	18	19	17	17	18	43	34
145	131	136	140	144	136	139	140	185	223
6	5	4	5	5	5	5	5	25	19
25	21	24	19	20	20	23	19	28	31
493	489	495	462	468	474	460	471	165	255
6	5	7	6	6	5	7	4	6	7
261	242	261	269	255	236	241	250	328	308
24	25	22	24	23	22	23	23	31	20
89	96	105	89	86	79	81	86	189	215
134	137	128	132	127	123	127	128	218	181

Table 6 (continued).

Core, section:	181R-3	181R-3	181R-3	182R-1	182R-2	182R-3	182R-3	183R-1	184R-1	184R-1	184R-2
Interval (cm):	15–18	38–41	91–96	3–6	99–102	3–6	48–51	143–146	18–21	64–66	109–111
SiO_2	46.22	46.01	45.91	46.96	47.04	46.52	46.54	46.89	47.54	46.95	48.58
TiO_2	2.52	2.30	2.26	2.19	2.16	2.24	2.21	3.19	3.19	3.34	2.84
Al_2O_3	16.77	15.44	15.39	14.85	15.2	15.14	14.84	15.04	15.31	16.29	15.46
Fe_2O_3	12.07	12.82	11.99	12.12	12.05	12.15	12.21	13.7	12.79	13.28	11.93
MnO	0.20	0.15	0.25	0.17	0.17	0.18	0.16	0.31	0.31	0.15	0.16
MgO	8.96	8.96	7.04	8.94	7.92	7.24	7.53	7.48	6.32	5.67	8.02
CaO	3.65	5.99	10.19	9.20	9.83	9.64	10.30	5.86	8.29	7.03	4.40
Na_2O	2.84	2.75	3.23	2.74	2.84	2.98	2.78	3.49	3.54	3.58	3.39
K_2O	2.25	1.53	0.54	0.51	0.51	0.50	0.49	0.74	0.64	0.72	1.35
P_2O_5	0.37	0.31	0.31	0.29	0.29	0.29	0.31	0.36	0.37	0.38	0.35
LOI	4.60	3.96	3.27	2.21	2.11	2.48	2.53	3.41	1.48	2.31	4.37
Total	100.45	100.22	100.38	100.18	100.12	99.36	99.90	100.47	99.78	99.70	100.85
Rare earth elements (in ppm) by ICP-MS:											
La	22.7	19.5	21.0	19.3	19.9	19.9	20.9	26.5	28.0	29.4	19.4
Ce	50.1	44.8	47.2	44.3	44.3	46.0	48.2	56.1	61.4	62.1	45.1
Pr	5.97	5.24	5.80	5.21	5.36	5.42	5.55	6.98	7.71	7.71	5.52
Nd	26.4	23.2	24.8	23.5	23.6	23.7	25.1	30.7	33.1	33.4	26.3
Sm	5.55	4.86	5.11	5.03	4.76	4.80	5.07	6.23	6.91	7.14	5.63
Eu	1.75	1.69	1.71	1.65	1.68	1.75	1.84	2.16	2.36	2.36	2.06
Tb	0.75	0.76	0.81	0.76	0.74	0.79	0.83	1.02	1.08	1.07	0.90
Ho	0.90	0.86	0.90	0.87	0.91	0.89	0.91	1.17	1.15	1.18	1.00
Er	2.52	2.37	2.61	2.52	2.45	2.32	2.53	3.21	3.07	3.22	2.66
Yb	2.07	2.01	2.10	2.11	2.04	2.08	2.21	2.61	2.64	2.86	2.15
Lu	0.29	0.32	0.28	0.26	0.31	0.30	0.29	0.34	0.40	0.42	0.27
Other trace elements (in ppm) by XRF:											
Ba	126	120	105	85	98	95	90	140	142	156	115
Co	58	56	52	54	54	48	54	56	51	55	53
Cr	388	341	289	325	314	300	300	174	167	173	206
Cu	82	86	105	91	74	79	72	53	65	80	37
Nb	37	34	33	32	31	33	32	46	46	50	35
Ni	227	221	235	221	222	216	210	121	110	118	140
Rb	17	7	12	11	11	11	12	12	13	15	13
Sc	35	26	26	27	25	25	25	29	30	34	27
Sr	275	344	380	337	370	368	357	411	437	466	360
Th	6	8	6	5	5	7	6	8	7	8	5
V	280	255	234	241	236	251	220	375	352	359	282
Y	27	25	27	25	25	25	25	29	31	30	26
Zn	125	81	113	95	95	96	86	113	111	114	101
Zr	193	174	171	164	165	169	165	227	224	236	199

Table 7. Whole-rock XRF and ICP-MS analyses of basaltic lavas from Hole 865A.

Core, section:	90R-3	91R-1	91R-2	91R-3	93R-2	93R-3	94R-1	94R-2	94R-4
Interval (cm):	102–106	128–130	69–71	20–23	14–17	86–89	91–94	31–34	134–131
SiO_2	43.33	44.13	43.95	43.71	43.53	45.80	45.01	42.98	46.11
TiO_2	3.35	3.65	3.74	3.60	3.66	3.67	3.59	3.73	3.30
Al_2O_3	15.84	18.30	18.04	17.64	16.16	15.78	16.00	16.00	15.99
Fe_2O_3	10.84	9.35	9.22	9.38	11.09	9.17	9.46	11.16	9.69
MnO	0.11	0.11	0.10	0.09	0.12	0.15	0.16	0.15	0.13
MgO	10.38	8.47	9.09	9.57	8.02	8.45	8.19	12.39	7.61
CaO	4.47	7.41	4.72	5.26	7.05	9.21	10.28	2.06	8.78
Na_2O	1.79	2.15	1.65	2.00	1.75	2.54	2.12	1.34	2.27
K_2O	1.73	0.90	2.05	1.35	2.72	1.17	1.12	2.51	2.25
P_2O_5	0.65	0.73	0.68	0.72	0.77	0.72	0.77	0.80	0.80
LOI	7.89	4.77	7.35	6.78	5.46	3.73	3.38	7.41	3.14
Total	100.38	99.97	100.59	100.10	100.33	100.39	100.08	100.53	100.07
Rare earth elements (in ppm) by ICP-MS:									
La	37.2	43.0	43.6	42.7	46.2	41.9	48.3	42.0	43.7
Ce	79.1	93.3	96.2	90.7	102.0	93.5	103.0	89.6	93.3
Pr	9.51	11.2	11.3	11.1	12.7	11.7	12.7	11.2	11.6
Nd	39.0	46.6	46.1	45.6	52.1	49.8	53.7	46.5	47.2
Sm	7.28	8.25	8.50	8.28	9.33	8.46	9.35	7.94	8.31
Eu	2.24	2.62	2.70	2.63	2.80	2.66	2.99	2.50	2.62
Tb	0.93	1.00	1.07	1.05	1.05	0.99	1.13	0.92	1.00
Ho	0.90	1.11	1.05	1.14	0.98	1.04	1.10	0.92	0.94
Er	2.37	2.99	2.72	3.05	2.63	2.84	2.93	2.40	2.50
Yb	2.08	2.24	2.23	2.37	2.11	2.22	2.35	2.10	2.10
Lu	0.28	0.30	0.34	0.33	0.30	0.29	0.33	0.34	0.29
Other trace elements (in ppm) by XRF:									
Ba	685	623	530	617	717	673	689	694	719
Co	56	48	44	45	49	41	46	55	39
Cr	231	239	267	259	191	179	188	227	154
Cu	67	52	50	51	37	46	48	95	42
Nb	78	86	88	86	75	74	75	78	76
Ni	194	159	152	156	130	111	130	129	133
Rb	19	9	17	11	48	13	12	25	43
Sc	30	35	36	38	25	27	26	34	18
Sr	526	797	562	711	668	742	827	383	748
Th	9	9	10	11	9	8	10	11	11
V	300	302	327	330	289	264	259	357	239
Y	23	30	28	30	29	27	27	28	27
Zn	85	87	126	92	81	75	78	74	79
Zr	324	354	365	351	350	346	342	364	361

Notes: Major oxides in weight percent (wt%) and trace elements in parts per million (ppm). LOI = loss on ignition.

Table 6 (continued).

185R-1 83–86	185R-2 62–66	185R-3 28–32	185R-3 88–92	186R-2 128–131	186R-3 12–15	188R-3 40–43	188R-4 29–31	189R-1 11–14	189R-1 66–69	189R-3 2–4	189R-4 11–14
48.00	47.47	47.93	47.60	47.04	46.17	44.90	46.25	45.73	46.06	48.26	47.07
2.77	2.25	2.71	2.82	3.44	3.17	2.28	2.01	2.03	2.08	2.12	2.40
15.58	15.81	15.09	15.96	16.40	15.87	14.26	12.85	13.13	13.36	14.69	16.87
11.57	11.32	12.21	12.44	12.84	13.44	12.50	12.13	12.49	12.91	10.35	10.35
0.21	0.18	0.18	0.25	0.12	0.15	0.17	0.22	0.18	0.20	0.24	0.27
6.38	6.30	6.54	5.52	6.50	6.75	12.99	11.09	11.24	10.79	11.36	9.01
9.03	10.68	9.07	9.06	6.48	8.29	5.52	9.65	9.35	9.42	4.18	5.71
3.30	3.12	3.11	3.33	3.41	3.41	2.62	2.03	2.06	2.16	2.60	3.04
0.55	0.47	0.54	0.60	1.00	0.73	0.44	0.35	0.37	0.36	1.41	1.13
0.37	0.31	0.36	0.39	0.41	0.39	0.23	0.20	0.20	0.22	0.28	0.33
2.78	2.53	2.30	1.97	2.47	1.94	4.35	3.58	3.09	2.26	5.04	3.89
100.54	100.44	100.04	99.94	100.11	100.31	100.26	100.36	99.87	99.82	100.53	100.07
19.9		20.4	22.0	31.9	31.5	16.0	15.4	16.0	16.1	18.2	21.3
47.6		46.8	50.5	70.2	71.5	36.4	33.8	35.3	36.0	42.8	50.0
6.07		6.05	6.27	8.45	8.41	4.38	4.15	4.32	4.50	5.14	6.12
27.5		27.5	28.7	36.9	36.6	18.9	18.7	19.4	19.1	23.8	28.0
6.06		5.94	6.37	6.88	7.32	3.98	3.91	3.99	4.28	5.03	5.77
2.08		2.09	2.25	2.32	2.39	1.28	1.35	1.36	1.46	1.67	2.03
0.93		0.90	0.97	0.95	1.07	0.67	0.66	0.67	0.69	0.77	0.91
1.07		1.06	1.09	1.08	1.10	0.71	0.83	0.71	0.78	0.89	1.01
2.91		2.95	2.92	2.96	2.99	2.13	2.21	2.15	2.01	2.47	2.72
2.43		2.22	2.40	2.35	2.71	1.82	1.87	1.75	1.83	1.99	2.26
0.29		0.36	0.33	0.37	0.38	0.27	0.30	0.25	0.31	0.32	0.33
104	100	102	108	175	149	72	68	87	76	76	126
47	46	56	46	54	54	75	65	63	65	57	53
286	188	203	211	213	211	639	643	488	470	353	313
43	42	63	54	77	72	75	67	78	73	68	63
32	28	34	33	58	52	29	24	24	26	28	32
143	200	159	154	133	135	348	363	343	358	198	181
8	7	9	9	6	9	5	6	7	7	6	6
24	16	23	28	28	31	45	32	26	23	28	35
417	434	408	449	500	491	296	266	284	294	306	403
5	6	7	6	7	7	6	6	6	8	6	9
272	189	247	261	335	306	321	264	272	252	263	267
29	24	29	31	28	32	22	22	21	22	24	26
109	84	107	105	104	103	111	88	91	91	110	184
182	159	196	197	285	257	145	126	126	132	188	214

Table 8. Least-squares mixing calculation results.

Parent	Daughter	Method	Σ	F (%)	Oliv (%)	Cpx (%)	Plag (%)	Tmag (%)	Ilm (%)	Orth[a] (%)	Comments
Hole 866A depleted lavas:											
180R-4, 1–4	180R-1, 132–136	Cumulative	0.02	73.5	7.4	3.7	13.1	2.4	—	—	Reasonable fit
179R-6, 10–13	180R-1, 132–136	Incremental	0.01	97.0	1.6	1.0	0.2	0.2	—	—	Reasonable fit
189R-1, 11–14	182R-3, 3–6	Cumulative	0.29	82.1	10.2	5.7	0.8	0.7	—	0.4	Reasonable fit
182R-2, 99–102	182R-3, 3–6	Incremental	0.01	92.2	2.3	1.7	2.7	—	—	0.6	Reasonable fit
Hole 866A mildly enriched lavas:											
189R-3, 2–4	185R-3, 88–92	Cumulative	2.70	12.0	29.0	—	41.8	4	3.3	13.9	Not good[b and c]
185R-1, 83–86	185R-3, 88–92	Incremental	0.09	73.2	4.9	5.4	13.9	—	1.0	1.6	Not good[c]
Hole 866A depleted and mildly enriched lavas:											
180R-4, 1–4	185R-1, 83–86	Cumulative	0.01	61.7	7.0	6.2	21.6	3.6	—	—	Reasonable fit
180R-4, 1–4	185R-3, 88–92	Cumulative	0.01	61.5	7.0	6.3	21.5	3.8	—	—	Reasonable fit
Hole 866A enriched and mildly enriched lavas:											
189R-1, 11–14	185R-1, 83–86	Cumulative	0.21	65.0	15.2	10.0	8.1	0.9	—	0.8	Not good[c]
189R-1, 11–14	185R-3, 88–92	Cumulative	0.16	62.5	16.8	10.9	8.6	—	—	1.1	Not good[c]
Hole 866A enriched and depleted lavas:											
189R-1, 11–14	179R-5, 51–59	Cumulative	1.28	74.3	11.6	9.4	—	1.7	—	2.9	Not good[b and c]
189R-1, 11–14	179R-6, 10–13	Cumulative	0.24	74.3	14.8	8.3	0.4	—	—	2.1	Not good[c]
180R-4, 1–4	866A-182R-2, 99–102	Cumulative	0.20	81.6	2.4	—	13.0	2.4	—	0.7	Not good[c]
180R-4, 1-4	182R-3, 3-6	Cumulative	0.12	79.8	3.8	—	13.9	2.1	—	0.4	Not good[c]
Hole 865A basalts:											
90R-3, 102–106	91R-1, 128–130	Cumulative	2.15	69.1	14.2	—	5.7	—	1.3	9.7	Not good[b and c]
91R-3, 20-23	91R-1, 128-130	Incremental	2.44	76.1	7.9	—	8.9	—	1.5	5.6	Not good[b and c]
90R-3, 102-106	94R-4, 134-131	Cumulative	4.80	4.8	26.8	—	51.0	—	8.4	9.1	Not good[b and c]
94R-1, 91-94	94R-4, 134-131	Incremental	0.07	56.7	6.2	10.8	23.1	—	3.2	—	Reasonable fit

Note: F (%) = amount of liquid remaining in the system after the removal of crystals. Oliv = olivine, Cpx = clinopyroxene, Plag = plagioclase, Tmag = titanomagnetite, Ilm = ilmenite, and Orth = orthoclase.

[a] Orthoclase is generally a secondary mineral and is usually not present in fresh mafic lavas.

[b] Large residual errors.

[c] Unlikely mineral assemblage.